Delft Breast Ultrasound

The development of a water-cup ultrasound breast scanning system

Ernest Janssen

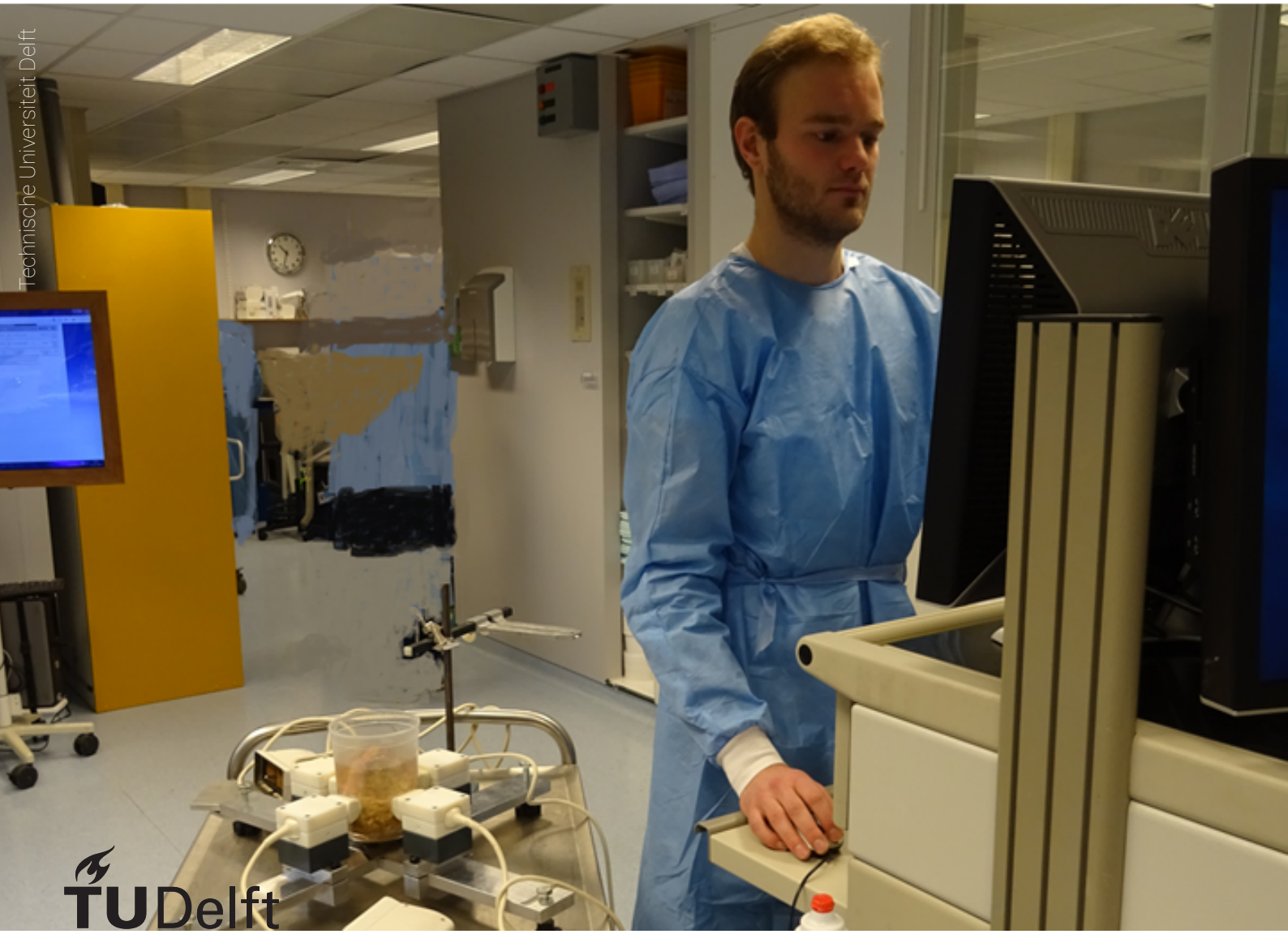

TU Delft

Delft Breast Ultrasound

The development of a water-cup ultrasound breast scanning system

by

Ernest Janssen

to obtain the degree of Master of Science
at the Delft University of Technology,
to be defended publicly on Wednesday March 13, 2019 at 10:00 AM.

Student number:	4246861	
Project duration:	March 23, 2018 – February 22, 2019	
Thesis committee:	Dr. ir. K. W. A. van Dongen,	TU Delft, supervisor
	U. Taskin, MSc.,	TU Delft, supervisor
	Prof. dr. ir. N. de Jong,	TU Delft & Erasmus MC
	Dr. N. Bhattacharya,	TU Delft

TU Delft

Abstract

Breast cancer is impacting over 1.5 million women each year. Early detection is essential in decreasing the mortality rate. Mammography is currently the golden standard for breast screening. However, this method is not ideal and water-bath ultrasound breast scanning is considered to be a promising screening modality. This type of scanning system is able to obtain ultrasound reflection and transmission data.
In this study, a water-cup breast scanning setup is built. The setup consists out of a plastic cup with four acoustic windows and four phased array ultrasound probes. The water-cup is used to execute a phantom study. The phantom study gives insight into the operability of the built water-cup. The differences between reflection and transmission data are observed and utilised. One imaging algorithm and two inversion algorithms are employed to reconstruct an image of the phantom. The images of the different algorithms are compared.
Furthermore, a method is proposed that reduces the computation time of a reflection data based Born inversion algorithm. In the end, the water-cup is used to image an ex-vivo human breast. Finally, the limitations of the built water-cup are stated.
In addition to manufacturing the water-cup, a pulse-echo-scan of an ex-vivo human breast is made. This pulse-echo-scan is compared with the cross-sectional photograph of the breast. Due to the pudding-like structure of the breast, it is challenging to make a cross-section at the same position as the pulse-echo-scan is made. The pulse-echo-scan is made at the Pathology Department of the Erasmus MC. The ex-vivo human breast study helps to understand what structures are present in the breast. This knowledge can be used to build a new measurement setup and optimize the imaging algorithms for finding tumours.

Ernest Janssen
Delft, February 2019

Contents

1 Introduction

Breast cancer is the second most diagnosed cancer among people worldwide and the most frequent cancer among women, impacting over 1.5 million women each year. It is well recognized that early detection is critical in decreasing the mortality rate of breast cancer [1, 2].
In the Netherlands, there is a two-yearly population screening on breast cancer for women between 50 and 75 years old. Mammography is currently used as breast scanning method [3].

1.1. Scanning modalities for breast cancer detection

There are various breast scanning methods available. The three main methods will be explained briefly.

- **Mammography** uses low-energy X-rays to scan the breast. X-ray is a form of electromagnetic radiation with frequencies in the range of 3×10^{16} Hz to 3×10^{19} Hz. The main drawbacks of using mammography as screening method are the dose of ionizing radiation used, the pressure of the scanning equipment is uncomfortable and the imaging resolution obtained is not optimal for young women with dense breasts.

- **Magnetic resonance imaging (MRI)** uses strong magnetic fields and radio frequency waves. In contrast to mammography, an MRI scanner does not use any ionizing radiation. The cost and complexity of an MRI scan are the main drawbacks. Also, people with metal parts in their body cannot be scanned applying MRI.

- **Ultrasound** is sound with frequencies higher than audible for humans. Sound waves with frequencies between 100 kHz and 10 MHz are used for medical imaging. Using ultrasound is relatively inexpensive compared to MRI, is not using ionizing radiation and is capable of imaging dense breasts typical for young women. Therefore ultrasound can be seen as a promising breast scanning method.

1.2. Ultrasound breast scanning

In order to image a breast using ultrasound, transducers are placed at different angles on or around the breast. Transducers are used to excite ultrasound waves. Multiple transmitter-receiver combinations are used to scan the breast. The difference in speed of sound and attenuation of breast tissue is used to image the breast and distinguish healthy breast tissue from tumours.

The ultrasound breast scanning systems can be divided into three groups: hand-held ultrasound (HHUS), automated breast volume scanner (ABVS) and the so-called water-bath method. The different setups will be explained briefly. Moreover, the advantages and disadvantages will be stated. For the water-bath setup, there is an extra focus on the development of the three systems described by Özmen [4].

Figure 1.1: An example of HHUS scanning. Reprinted from Breast Imaging, from http://www.valleyradiologists.com/breast-imaging.php?pID=5.

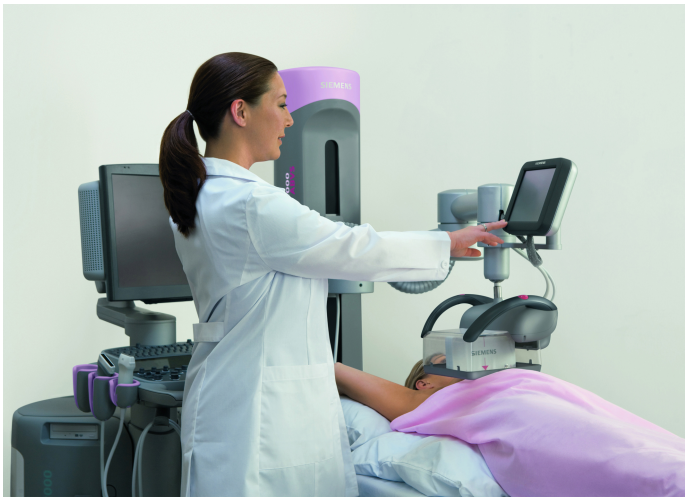

Figure 1.2: An example of an ABVS. Reprinted from Breast Imaging, from http://www.valleyradiologists.com/breast-imaging.php?pID=5.

- **Hand-Held UltraSound (HHUS)** is being used as an extra imaging tool besides mammography for breast cancer detection. Figure 1.1 shows an example of an HHUS scanner. The scan is made with frequencies in the range of 5 to 15 MHz [5]. It has the advantage of real-time imaging. The disadvantages are the operator dependency, deformation of the breast when scanning, the duration of examination, only pulse-echo data is obtained and the scan is not reproducible.

- **Automated Breast Volume Scanner (ABVS)** is an ultrasound device with a wide aperture which is pressed against the breast to scan the breast in a sweep. Figure 1.2 shows an ABVS system; the Acuson S2000 developed by Siemens Medical Solutions. The scanning head can be tilted to scan the breast under multiple angles. It employs frequencies in the range of 5 to 14 MHz. The measured data is saved and processed to make multiplanar images of the breast. The advantage of this method is that it is less operator dependent compared to HHUS, it shows reproducible results and it is able to image axial, sagittal, and coronal planes of the breast. The disadvantage is the deformation of the breast during the scan, the scanning time is long and only pulse-echo data is obtained.

- **Water-bath scanning method** includes an examination bed with an opening to a water bath. Figure 1.3 shows an example of a water bath scanner setup. The water functions as an acoustic coupling medium between the ultrasound transducer and the breast. During the scan, the breast will be measured at multiple angles. The advantages of this method are: the minimal deformation of the breast during the

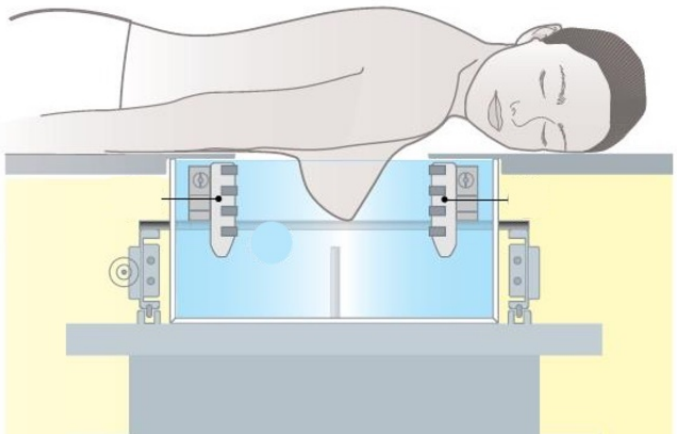

Figure 1.3: An example of a water-bath ultrasound breast scanner. Reprinted from BEATING BREAST CANCER by Susan Misicka, from https://www.swissinfo.ch/eng/sci-tech/beating-breast-cancer-could-an-ultrasound-bath-squeeze-out-mammograms-/38394752.

measurement, the breast can be viewed from different angles all around the breast which implies that transmission and reflection signals can be obtained and this scanning method is operator independent. The disadvantage can be a long scanning time and the setup must correct for patient movement.

1.2.1. Water-bath ultrasound scanning systems

In this section, an overview is given of different water-bath setups developed by research groups around the world. The features of the three leading water-bath systems are considered and their development since the publication of Özmen's PhD thesis. The main factors on which the comparison of the systems is made are: the type of imaging algorithm and the scanning design. Including: the transmitted centre frequency, the time to reconstruct an image, the number of transducers (sources and receivers) and the geometry of the system f.e. scanning in 2D or 3D. Besides the three systems that are shown in Özmen's thesis, there are five other scanning setups reviewed. Six of these scanning machines have scanned in-vivo human breasts. The other two are showed to compare the scanner design considerations.

- **SoftVue**: The SoftVue system is a water-bath system developed by Duric et al. [6]. Figure 1.4 shows the system. It uses a ring-shaped array to scan the breast, also shown in Figure 1.4. The ring has a diameter of 22 cm and consists of 2048 transducer elements, where 256 transducer elements are being used to minimize reconstruction time [7]. The transducers operate at a centre frequency of 1.5 MHz. Whereas a signal bandwidth of 0.4 to 1 MHz is used to reconstruct a speed-of-sound profile, the resolution is approximately 1.5 mm.

  In-vivo measurements have been used to compare a ray-based reconstruction technique with a waveform reconstruction technique. Figure 1.5 shows the improved resolution using a waveform reconstruction algorithm. The waveform reconstruction technique is based on the principles of full-wave

Figure 1.4: SoftVue scanning system

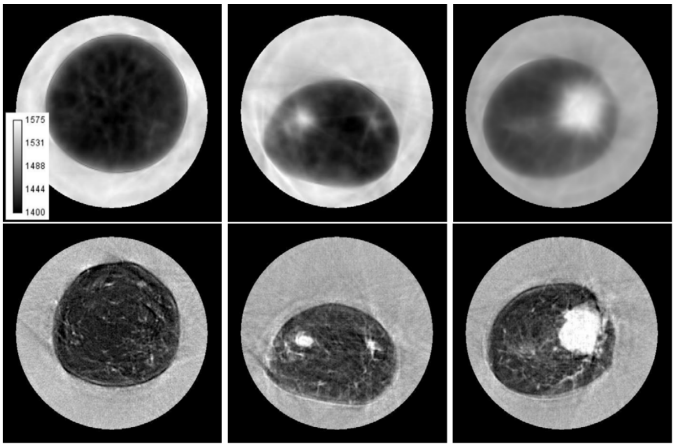

Figure 1.5: Comparison of ray-based and waveform reconstruction methods. Top row images are reconstructed using ray-based method. Bottom row images are reconstructed using a waveform-based reconstruction method. The gray scale is a speed of sound scale from 1400 m/s - 1575 m/s

inversion, operates in the frequency domain and uses a gradient descent method to reconstruct an image [8].

- **CVUS (computerized volumetric ultrasound)**: The CVUS-system is developed by Wiskin et al. Figure 1.6 shows the system. It consists of a transmitter, a receiver and three reflection arrays with different focal length. The transmitter and receiver arrays have 8 rows by 192 columns containing 1536 elements to collect transmission data. The transmission transducers use a chirp signal generally spaced from 0.3 to 1.3 MHz. The reflection data is obtained with a pulse of 4 MHz. The data is collected on horizontal levels, each level is 2 mm apart. At each level, the transducer system is rotated horizontally over 180° [9].

  A paraxial approximation of the Helmholtz equation is used for a wave-based reconstruction algorithm.

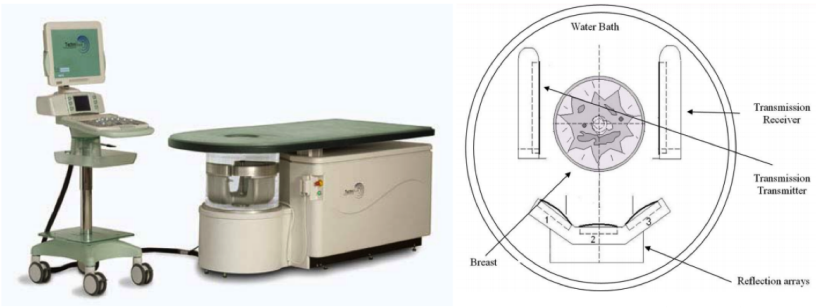

Figure 1.6: CVUS scanning system

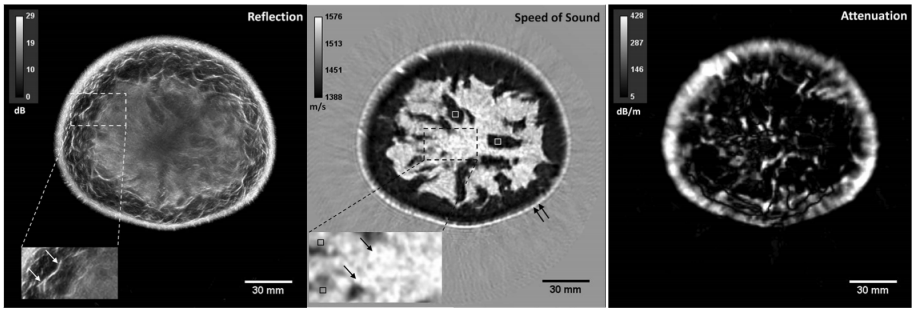

Figure 1.7: Reflection, speed of sound and attenuation images obtained with the CVUS-system

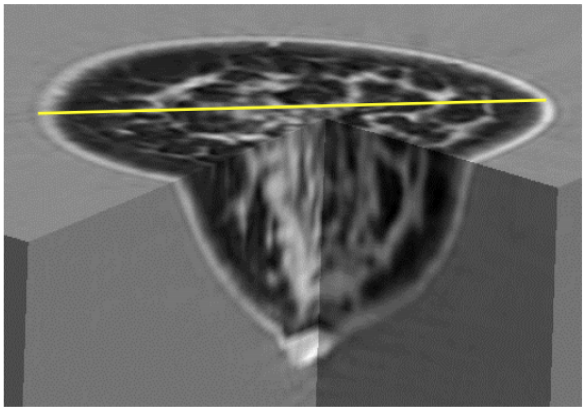

Figure 1.8: 3D breast image obtained with the CVUS system. On the grayscale the light colour represents high speed of sound.The yellow line indicates a diameter of 106mm

A resolution of 1 mm is achieved with a scanning time of approximately 7 min. per breast. Whereas the reconstruction algorithm takes about 35 min. Up to date, at least 500 breasts are scanned by this system. The CVUS system is able to compute speed of sound, attenuation and reflection images [10]. Figure 1.7 shows images that are obtained with the CVUS-system.

Figure 1.8 shows a 3D breast image computed by the CVUS system. The CVUS system is a 2D scanning system, this can be seen in Figure 1.8, whereas the coronal plane image has a higher resolution than the sagittal and transverse plane images. This is caused by the out of plane scattering occurring in a 2D scanning system.

- **KIT 3D USCT II**: the KIT 3D USCT is a water-bath system developed at the Karlsruhe Institute of Technology. Figure 1.9 shows the system. The scanning setup is formed by a semi-elliptical aperture with a diameter of 26 cm and a height of 18 cm. The aperture has 628 transmitters and 1413 receivers. Approximate spherical wavefronts at 2.5 MHz are generated by each transmitter. The first in-vivo results are obtained using a ray-based reconstruction algorithm. The spatial resolution of the speed of sound and attenuation images are in the range of 5 to 12 mm. The data acquisition takes about 6 min. per breast. To increase the resolution this group is focusing more on wave-based reconstruction methods [11, 12]. Figure 1.10 shows an image obtained with the KIT 3D USCT setup and an MRI image. The image is obtained by overlapping the reflection image with a speed of sound and an attenuation image, where the speed of sound and attenuation values are above a given threshold.

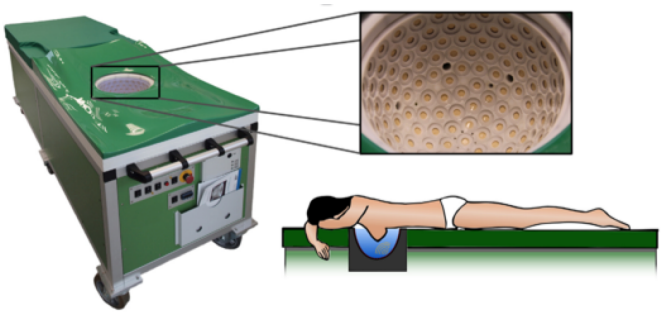

Figure 1.9: 3D USCT II scanning system

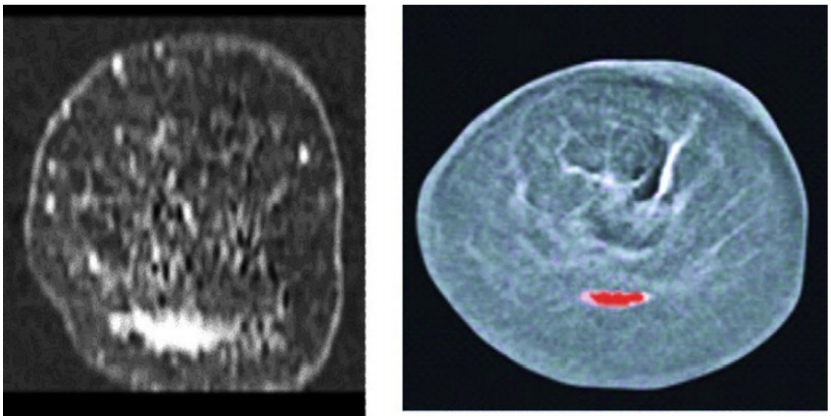

Figure 1.10: Image of left breast of a 74-year-old patient with large breast cancer. Left: a frontal MRI subtraction slice. Right: reflectivity image obtained with the KIT 3D USCT scanner. The red mark corresponds to a high speed of sound and attenuation level.

- **Los Alamos setup**: the Los Alamos National Laboratory developed the setup shown in Figure 1.11. This setup consists of two parallel linear transducer arrays with a total of 768 transducer elements and 384 parallel receive channels. The system is operating at a frequency of 1.875 MHz. Furthermore, the distance between the two transducer arrays is adjustable for scanning different sizes of breast [13]. The setup is using ultrasound bent-ray tomography to build an image. It takes approximately 2 min. for the Los Alamos system to scan a breast. Figure 1.12 shows an image obtained by the Los Alamos setup.

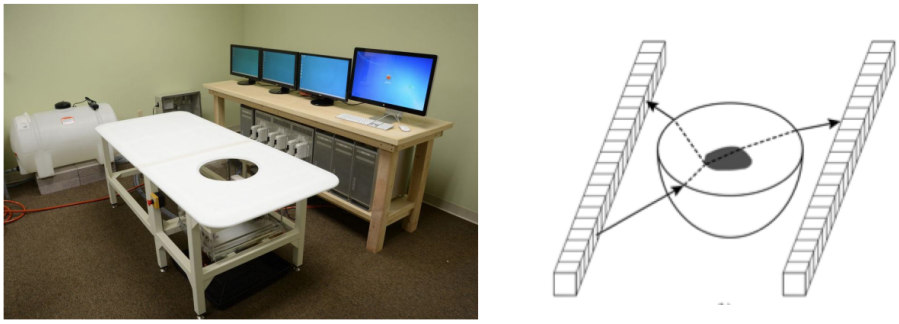

Figure 1.11: Los Alamos water-bath setup

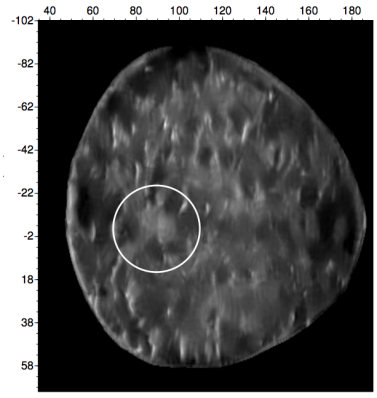

Figure 1.12: A coronal section breast image obtained by synthetic aperture beam-forming. With in the circle a breast lesion

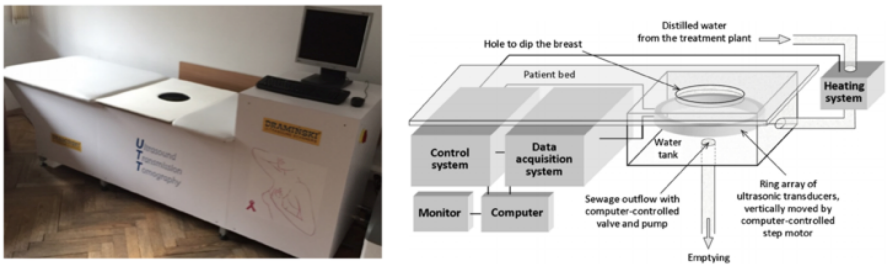

Figure 1.13: The UTSM by Wroclaw University

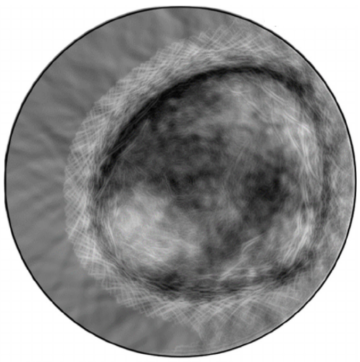

Figure 1.14: Ultrasound tomography image of the left breast of a patient (32 years) with glandular cancer. Light color indicates higher speed of sound values. The light colored spot at 8 o'clock is a cancer lump.

- **UTSM (ultrasound tomography scanner model)**: at the Wroclaw University, S.A. Dramínski developed the UTSM shown in Figure 1.13. This system comprises 1024 piezoceramic transducers distributed over a ring-shaped array, operating at a centre frequency of circa 2 MHz. This ultrasonic ring has a diameter of 260 mm and moves vertically, scanning coronal breast sections at 1 mm slice intervals. The time needed to scan a breast varies from 10 to 20 minutes depending on the breast length [14].

  Transmission images are produced using FBP (Filtered Back Projection) and reflection images with SAFT (Synthetic Aperture Focusing Technique). Figure 1.14 shows a coronal breast image obtained with the UST system developed at the University of Wroclaw. The image is built by overlaying transmission and reflection data.

- **BUTIS (breast ultrasound tomography imaging system)**: at the Huazhong University of Science and Technology, the BUTIS is developed. Figure 1.15 shows the BUTIS. The ring-shaped setup contains 1024 transducer elements operating at a centre frequency of 2.25 MHz [15].

Figure 1.15: Breast Ultrasound Tomography Imaging System (BUTIS) developed by the Medical Ultrasound Laboratory in HUST (Huazhong University of Science and Technology)

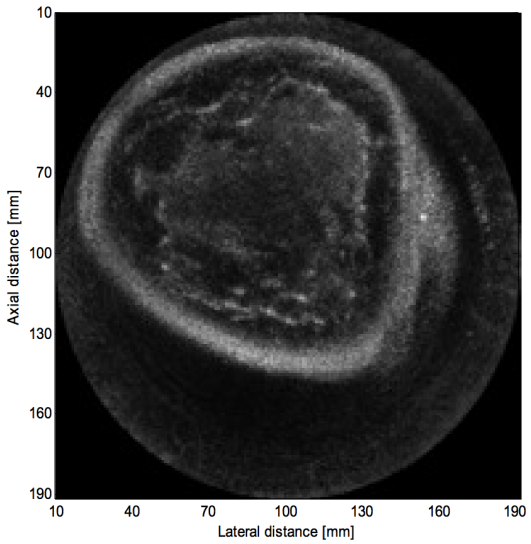

Figure 1.16: Example of breast image of a female volunteer obtained by the BUTIS in HUST. The image is constructed using a delay-and-sum method

Figure 1.16 shows an example of a breast image obtained by the BUTIS. The BUTIS setup uses a delay-and-sum method to reconstruct its images.

The above-described systems are the systems that have scanned in-vivo breast of patients. The following systems have not scanned any patients. The systems are discussed to show what setup is used and what imaging algorithms are used.

- **MUBI**: in Spain, the Multi-Modal Ultrasound Breast Imaging (MUBI) system is developed. Figure 1.17 shows the MUBI setup. This system consists of two linear arrays of 3.2 MHz and 5 MHz containing 128 elements. The transducer arrays are attached to independent arms moved by a stepper motor with a mechanical resolution of 0.1°. At the time this research group is developing a ring-shaped setup consisting of 16 phased-array transducers of 128 elements. The focus is on a full wave inversion reconstruction algorithm to obtain speed of sound and attenuation profiles [16].

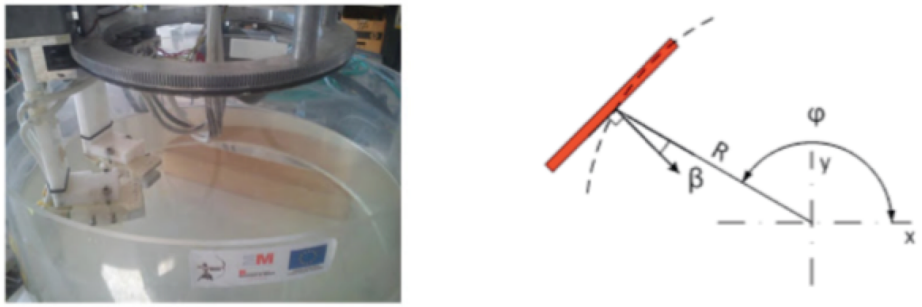

Figure 1.17: The Multi-Modal Ultrasound Breast Imaging (MUBI) system setup

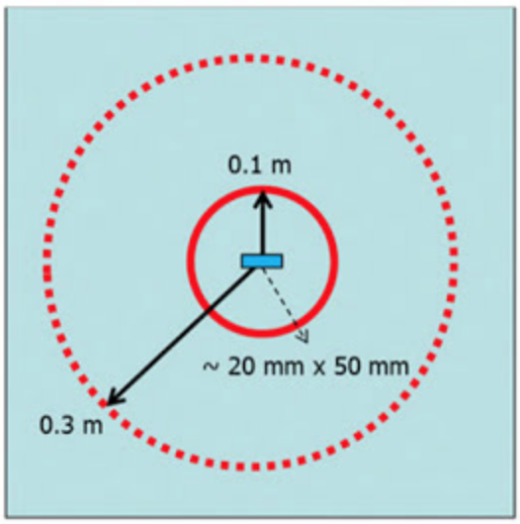

Figure 1.18: The DBUS setup. A 2D scanning system with two single transducers operating at a centre frequency of 0.5 MHz, with a transmitter radius of 0.3 m and a receiver radius of 0.1 m

- **DBUS**: during the Delft Breast Ultrasound Scanner project, a system is built including a water-tank and two 0.5 MHz transducers. One fixed transducer acts as a source and is connected to an arbitrary waveform generator. Whereas the other transducer is acting as the receiver and can be circularly rotated. Figure 1.18 shows the DBUS setup [17].

1.2.2. Discussion

In this section, the different setup methods are compared. The results of the comparison can be used for the development of the DBUS. There is a focus on the water-bath systems as these setups are operator independent, minimize the breast deformation while scanning and can measure both transmission and reflection signals for image reconstruction. For these systems, the aperture setups and the imaging algorithms are compared. In Table 1.1 the setup configurations are listed.

- **Centre frequency**: the centre frequencies are varying from 0.5 to 5 MHz. Usually, the lower centre frequencies indicate that a wave-based reconstruction algorithm is used.

- **2D/3D scanning setup**: the KIT 3D USCT scanner is the only system that takes 3D scattering into account, whereas ring-shape setups loose information due to the out of plane scattering. The disadvantages of a 3D setup are: data processing for this 3D system is geometrically more complicated, more electronics are required and the computation time is higher.

Table 1.1: Comparison of breast scanning setups

	$\mathbf{f_c}$	$\#_{\mathbf{transducers}}$	**2D/3D**
SoftVue	1.5 MHz	2048	2D
CVUS	4 MHz and 0.3-2 MHz	192 and 1024	2D
KIT 3D USCT II	2.5 Mhz	2041	3D
Los Alamos setup	1.875 Mhz	1152	2D
UTSM Wroclaw university	2 MHz	1024	2D
BUTIS	2.25 MHz	1024	2D
MUBI	3.2-5 MHz	128	2D
DBUS	0.5 MHz	2	2D

- **Imaging algorithm**: for the image reconstruction algorithm it can be seen that there is a shift from the ray-based methods to the full-wave inversion methods. Whereas the waveform based methods result in a better speed of sound estimations of the scanned tissue; the ray-based methods do physical assumptions that reduce the image resolution [8]. The full-wave inversion methods operate at lower frequencies due to the computational cost; scanning using a higher frequency bandwidth results in a larger data-set and a denser discretisation.

There are many variables to take into account when building a scanning system: number of transducers, centre frequency of transmitted signal, 2D or 3D scanning geometry, circular, elliptical or square transducer arrays. And for the image reconstruction and data processing: use of transmission and, or reflection data, use of a ray-based or a wave-based reconstruction technique. All these variables have an influence on the resulting resolution of the image and the reconstruction time.

1.3. Aim of this study

This project is part of the Delft Breast Ultrasound Scanner (DBUS) project. The DBUS project aims to develop an ultrasound breast scanner for detecting breast cancer. The current scanning system that is available for the DBUS project is not able to measure ex- or in-vivo human breast tissue, due to the size of the system, the data acquisition time and the measuring setup orientation.
This study is the start of practical work using a Verasonic Vantage 256 system to measure ex-vivo human breast tissue. The aim of this study is to:

- build a water-cup measurement system that can obtain transmission and reflection data,
- use the built water-cup setup to perform a phantom study that includes: a comparison of three types of imaging algorithms and differentiation between reflection and transmission signal,
- make an pulse-echo-scan of an ex-vivo human breast and compare this pulse-echo image with a cross-sectional photo of the breast.

1.4. Thesis outline

Firstly, in the Introduction various water-bath ultrasound scanning systems are compared. Next, the theory describing acoustic wave propagation and acoustic imaging is presented. In the experimental setup, there is a short introduction to the Verasonics research platform and properties of transducers are explained. In addition, the measurement and the imaging procedure for the built water-cup setup are explained and the method for comparing an ultrasound pulse-echo-scan with the cross-sectional photo of an ex-vivo human breast is presented. The results section shows a comparison of three imaging algorithms for the water-cup setup, it also demonstrates that inversion based images can be improved when transmission data and randomly picked frequencies for reflection data are scaled. Furthermore, a comparison of an pulse-echo-scan of an ex-vivo human breast with a cross-sectional photo is given. The final result is an image of an ex-vivo human breast measured with the four-probe water-cup setup. At the end of the thesis, the results are discussed and a conclusion is drawn. The conclusion includes advice for possible further research.

2

Theory

This chapter gives the theoretical background about the physical principles of medical diagnostic ultrasound. Firstly the basic principles of ultrasound propagating through heterogeneous media are given. Secondly, the acoustic wave equation is derived. Thirdly, three image reconstruction algorithms are explained. The goal of this chapter is to give a clear overview of the physical phenomena and theory used with breast ultrasound.

2.1. Ultrasound propagation

Ultrasound waves are excited by transducers. When ultrasound is propagating through media, several phenomena are taking place. There are waves that travel back to the transducer, called echoes. These waves are formed by reflections and scattering. The echoes are formed by differences in the acoustic impedance in the media. The acoustic impedance Z is an acoustic property that depends on the density ρ (kg/m^3) and speed of sound c (m/s) of the media and are related by Z=ρc (kg/m^2/s). Reflections occur when the wavelength of the incoming ultrasound wave is small compared to the interface with dissimilar impedance. For reflections, the reflection angle is the same as the angle of incidence. When reflection occurs there is also a part of the ultrasound wave transmitted through the interface. This transmitted part gets refracted, thus travelling in a different direction, when the incident wave propagates not perpendicular to the interface. Scattering takes place when the wavelength is large compared to the interface structure. The scattering phenomenon can be best visualized by light hitting the tip of a needle, the light gets scattered in all directions. Figure 2.1 shows the different propagation behaviours of ultrasound.

When ultrasound is propagating through a medium, mechanical energy is converted to heat. This is called absorption. The above-described phenomena, causing a loss in intensity of the forward propagating pulse, are all referred to attenuation. Attenuation is a frequency dependent effect and gives rise to dispersion. Intensity I is a measure of the power through a given cross-section in W/m^2. For a plane wave it is expressed as the particle velocity u multiplied with the pressure p, $I = pu = p^2/Z$. Where $Z = p/u$ is the acoustic impedance of the medium.

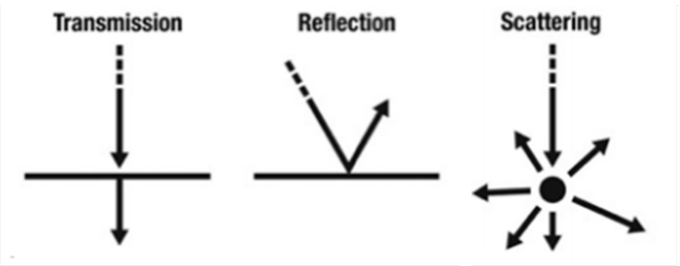

Figure 2.1: Overview of various behaviour of ultrasound wave propagation. Reprinted from Govers's MSc thesis. [18]

2.2. Acoustic wave equations

In this section, the theory of ultrasound and acoustic waves, is presented. The imaging and inversion algorithms are typically derived from these acoustic wave equations. The change of the acoustic pressure (p) and the particle velocity (v) as a function of space ($\vec{r}$) and time (t) is described by the acoustic wave equations. With the derivation of this equation, there are several approximations made. Here it is explained why these approximations can be made. More in-depth derivation and explanation of the derived equations can be found in the book of Gisolf and Verschuur.[19]

To derive expressions for the pressure and velocity we start with the equation of deformation, also called Hooke's law

$$\frac{\partial p(\vec{r},t)}{\partial t} = -\frac{1}{\kappa}\nabla\cdot\vec{v}(\vec{r},t) + \frac{1}{\kappa}q(\vec{r},t), \tag{2.1}$$

where $p(\vec{r},t)$ is the acoustic pressure; a scalar depending on space and time, $\vec{v}(\vec{r},t)$ is the particle velocity; a vector depending on space and time, κ is the compressibility and $q(\vec{r},t)$ is a volume source density of injection rate in s^{-1}.

The other acoustic field equation is the equation of motion, also called Newton's law

$$\nabla p(\vec{r},t) = -\rho\frac{\partial\vec{v}(\vec{r},t)}{\partial t} + \vec{f}(\vec{r},t) \tag{2.2}$$

where ρ is the volume density of mass and $\vec{f}(\vec{r},t)$ is a volume source density of force in $\mathrm{N/m}^3$.

In the absence of sources these two acoustic field equations can be combined to find the homogeneous acoustic wave equation. When the partial time derivative of the equation of deformation is combined with the divergence of the equation of motion, the resulting expression equals

$$\nabla^2 p(\vec{r},t) - \rho\kappa\frac{\partial^2 p(\vec{r},t)}{\partial t^2} = 0. \tag{2.3}$$

Note that $\rho\kappa = 1/c^2$, where c is the acoustic propagation velocity. Equation (2.3) is the linear homogeneous acoustic wave equation. In deriving this equation there were three linearizations applied: the volume density of mass ρ and the compressibility κ are taken to be pressure independent and the convection term of the material derivative is negelected. These approximations can be made when the amplitude of the pressure field is low. For the applications described in this thesis this is typically the case. When the medium parameters ρ and κ are constant in the medium this leads to an homogeneous wave equation.
Using a temporal Fourier transform of the form

$$\hat{g}(\vec{r},\omega) = \int_{-\infty}^{\infty} g(\vec{r},t)e^{-i\omega t}\,dt, \tag{2.4}$$

equation (2.3) can be expressed in the frequency domain as

$$\nabla^2\hat{p}(\vec{r},\omega) + \frac{\omega^2}{c^2}\hat{p}(\vec{r},\omega) = 0 \tag{2.5}$$

Equation (2.5) is called the Helmholtz equation. Where the caret symbol $\hat{\cdot}$ embodies a Fourier transform of the variable.
In biological tissue ρ and κ are typically not homogeneous. For heterogeneous media the acoustic medium parameters ρ and κ become spatially varying. Therefore Hooke's law is expressed as

$$\kappa(\vec{r})\frac{\partial p(\vec{r},t)}{\partial t} = -\nabla\cdot\vec{v}(\vec{r},t) + q(\vec{r},t) \tag{2.6}$$

and Newton's law

$$\nabla p(\vec{r},t) = -\rho(\vec{r})\frac{\partial\vec{v}(\vec{r},t)}{\partial t} + \vec{f}(\vec{r},t). \tag{2.7}$$

Combining the above equations and assuming constant density yield the heterogeneous acoustic wave equation

$$\nabla^2 p(\vec{r},t) - \frac{1}{c_0^2}\frac{\partial^2 p(\vec{r},t)}{\partial t^2} = -S_{pr}(\vec{r},t) - S_{cs}(\vec{r},t) \tag{2.8}$$

where $S_{pr}(\vec{r},t) = \rho_0 \partial_t q(\vec{r},t) - \nabla \vec{f}(\vec{r},t)$ and $S_{cs}(\vec{r},t) = (\frac{1}{c_0^2} - \frac{1}{c^2(\vec{r})})\partial_t^2 p(\vec{r},t)$ and the properties ρ_0 , c_0 refer to a homogeneous background medium. In deriving equation (2.8) the convection term in the material derivative is neglected.

Equation (2.8) is expressed in the frequency domain as

$$\nabla^2 \hat{p}(\vec{r},\omega) + \frac{\omega^2}{c_0^2}\hat{p}(\vec{r},\omega) = -\hat{S}_{pr}(\vec{r},\omega) - \hat{S}_{cs}(\vec{r},\omega). \tag{2.9}$$

This equation is known as the Helmholtz equation for heterogeneous media. A solution for this equation is a Green's function. The Green's function represents the impulse response of the medium. The Green's function for the 2D acoustic wave equation for homogeneous media is a second order Hankel function

$$\hat{G}(\vec{r},\omega) = \frac{i}{4} H_0^{(2)}\left(\frac{\omega}{c_0}|\vec{r}|\right), \tag{2.10}$$

with angular frequency ω.

The total pressure field $\hat{p}(\vec{r},\omega)$ in heterogeneous media can be expressed as a summation of the incident field $\hat{p}^{inc}(\vec{r},\omega)$ and the scattered field $\hat{p}^{sct}(\vec{r},\omega)$. In this formalism the incident field is defined as the field generated by the primary sources and propagating through the homogeneous background medium. The scattered field may be understood as a correction term to the incident field to yield the total field. Consequently, the total pressure field is a linear combination of both and equals

$$\hat{p}(\vec{r},\omega) = \hat{p}^{inc}(\vec{r},\omega) + \hat{p}^{sct}(\vec{r},\omega) \tag{2.11}$$

where

$$\hat{p}^{inc}(\vec{r},\omega) = i\omega\rho_0 \int_{\vec{r}'\in D} \hat{G}\left(\vec{r}-\vec{r}',\omega\right)\hat{q}\left(\vec{r}',\omega\right) dV\left(\vec{r}'\right). \tag{2.12}$$

Thus the incident field at a point in space is generated by convolving the source term $\hat{q}\left(\vec{r}',\omega\right)$ with the Green's function $\hat{G}\left(\vec{r}-\vec{r}',\omega\right)$.
Furthermore, assuming density to be constant and the medium to be lossless, the Fredholm integral equation of second kind is derived

$$\hat{p}^{sct}(\vec{r},\omega) = \omega^2 \int_{\vec{r}'\in D} \hat{G}\left(\vec{r}-\vec{r}',\omega\right)\chi(\vec{r}')\hat{p}(\vec{r}',\omega) dV\left(\vec{r}'\right) \tag{2.13}$$

where $\chi(\vec{r}') = \frac{1}{c^2(\vec{r}')} - \frac{1}{c_0^2}$. Equation (2.13) can be explained by arguing that each contrast acts as a source generating an acoustic field.

2.3. Imaging and inversion methods

The ultrasound field that is tansmitted into the biological tissue propates through the tissue or gets reflected. The transmission and reflection signals can be measured using transducers. The measured signals are used to make an image of the tissue. The term imaging is typically used as a direct method aiming at localizing contrasts, whereas inversion is often an iterative method used for reconstructing acoustic medium parameters. In this section, there are three reconstruction methods explained. **SAFT** (Synthetic Aperture Focusing Technique) is an imaging method that is also known as time-domain migration or delay-and-sum imaging, **ART** (Algebraic Reconstruction Technique) is an iterative tomographic method and **BI** (Born inversion) is an inversion method that solves a linearized version of (2.13).

2.3.1. SAFT

Synthetic Aperture Focusing Technique is a wave based reflection imaging technique. This method is useful when boundaries of objects need to be detected. The method does not take multiple scattering into account and does not correct for geometrical spreading. It constructs an image by determining the time it takes for the ultrasound wave to travel from a source at $\vec{r}^{\,src}$ to a receiver at $\vec{r}^{\,rcv}$ via a boundary. By summing the reflection signals of all the source-receiver combinations an image is formed. Thus a contrast function is formed by

$$\chi(\vec{r}) = \sum_{src,rec} p^{sct}_{src,rec}\delta\left(\vec{r}^{\,rcv}, t = \frac{\|\vec{r}^{\,rcv} - \vec{r}\|}{c_0} + \frac{\|\vec{r} - r^{\,src}\|}{c_0}\right). \tag{2.14}$$

In equation (2.14) there is a summation of the measured field for all the source-receiver combinations. The δ-function describes a Dirac-delta peak at $t = \frac{\|\vec{r}^{\,rcv} - \vec{r}\|}{c_0} + \frac{\|\vec{r} - r^{\,src}\|}{c_0}$.

2.3.2. ART

Algebraic Reconstruction Technique is a ray-based imaging method. The method uses transmission signals to reconstruct a speed of sound profile of a medium. The phase shifts between an empty measurement and a phantom measurement are used to reconstruct an image and are obtained using cross-correlation. The method can be formulated as follows

$$Ax = b \tag{2.15}$$

where A is an M×N matrix, x is a vector of length N and b is a vector of length M. N is the number of grid points of the image and M is the number of measurements. A contains weighting values for each grid point, based on the length of the ray that passes the grid-point. x is the unknown slowness from which a speed of sound map of the image is derived and b consists of the phase shifts of each measurement. Because the matrix A of equation (2.15) is large, the following iterative scheme is used to solve for the slowness x.

$$x^{(k+1)} = x^{(k)} + \lambda^{(k)}\frac{(b_i - r_i x^{(k)})}{\|r_i\|_2^2} r_i \tag{2.16}$$

where k is the iteration number, λ is the regulation parameter, r_i is the ith row of A, b_i is the ith measurement and $\|r_i\|_2^2$ is the L2-norm of the r_i vector.[20]

2.3.3. BI

Starting from equation (2.13) the Born approximation is applied. The Born approximation is a linearization process that results in neglecting multiple scattering. This implies that the total field $\hat{p}(\vec{r}',\omega)$ within the integrand is replaced by the incident field $\hat{p}^{inc}(\vec{r}',\omega)$. The result is

$$\hat{p}^{sct}(\vec{r},\omega) = \omega^2 \int_{\vec{r}\in D} \hat{G}\left(\vec{r} - \vec{r}',\omega\right)\chi(\vec{r}')\hat{p}^{inc}(\vec{r}',\omega)dV\left(\vec{r}'\right). \tag{2.17}$$

In operator form equation (2.17) can be written as

$$\hat{p}^{sct}_j = M[\chi]. \tag{2.18}$$

Obtaining the adjoint of the operator, the expression for χ^{BP} is found

$$\chi^{BP} = \sum_{j,\omega} M^{\dagger}[\hat{p}^{sct}_j] = \sum_{\vec{r},j,\omega} \omega^2\{\hat{G}\left(\vec{r} - \vec{r}',\omega\right)\hat{p}^{inc}_j(\vec{r}',\omega)\}^*\hat{p}^{sct}_j(\vec{r},\omega). \tag{2.19}$$

Equation (2.17) is solved iteratively using Born inversion. In the first iteration step of the Born inversion, a model is built. This model is the same as an image constructed with the back-propagation algorithm. Each iteration the difference between the modeled and the measured data is calculated and this error is used to update the model. A schematic display of the iterative method is given by Table 2.1, the scheme is reprinted from Özmens [4].

Table 2.1: Born inversion scheme based on conjugate gradient iterative method

$\chi_0 = 0$

$\hat{r}_{j,0} = \hat{p}_j^{sct} - M[\chi_0]$

$\eta_1 = 0$

for n = 1,2,...

$g_n = M^{\dagger}[\hat{r}_{j,n-1}]$

$\eta_n = \|g_n\|_{\mathbb{D}}^2 \ / \ \|g_{n-1}\|_{\mathbb{D}}^2$

$d_n = g_n + \eta_n d_{n-1}$

$\alpha_n = \|g_n\|_{\mathbb{D}}^2 \ / \ \|M[d_n]\|_{\mathbb{S}}^2$

$\chi_n = \chi_{n-1} + \alpha_n d_n$

$\hat{r}_{j,n} = \hat{p}_j^{sct} - M[\chi_n]$

$E_n = \|\hat{r}_{j,n}\|_{\mathbb{S}} \ / \ \|\hat{p}_j^{sct}\|_{\mathbb{S}}$

if $E_n < \epsilon$ or $n > n_{max}$ stop

end

The BI scheme presented in Table 2.1 shows three times the operator M and once the adjoint operator $M^{\dagger}$. The operator M works on a contrast image. It simulates the data that is measured from a contrast image. The adjoint operator $M^{\dagger}$ reconstructs a contrast image from the measured data. The L_2-norm over the measured data space $\mathbb{S}$ and the image space $\mathbb{D}$ are denoted as $\|.\|_{\mathbb{S}}^2$ and $\|.\|_{\mathbb{D}}^2$ respectively. Furthermore, $\hat{r}_{j,n}$ is the error function that is minimized.

3

Experimental setup

During this project, two types of measurements are performed. A combined pulse-echo and tomographic scan is made of an agar phantom with a straw and two wires. In addition, a pulse-echo-scan of an ex-vivo human breast is made. Both setups are driven by a Verasonics Vantage 256 system. In this chapter, some properties of the Verasonics system are described and a description of the type of transducers that are used is given. Next, the water-cup setup, for obtaining pulse-echo and tomographic data, is explained. The data of the water-cup measurement is processed using three different imaging methods. There are also different configurations of Born inversion applied and these are explained. The chapter concludes with the procedure of the measurements on ex-vivo human breasts at the Pathology Department at the Erasmus MC.

3.1. Verasonics

The Verasonics Vantage 256 is a ultrasound research system driven by MATLAB. The system supports transmit frequencies down to 0.6345 MHz. The capability to transmit these low frequencies is important for the inversion algorithms, whereas the computation time of these algorithms depends on the frequency level. The system has two connectors that can accommodate two probes with a maximum of 128 elements each. Figure 3.1 shows the Verasonics Vantage 256.

3.1.1. Transducers

Transducers are used to transmit and receive ultrasound. A transducer consists of a piezo-electric element. Applying an oscillating voltage across the element causes it to vibrate and to transmit an ultrasound wave. This process transforms electrical into mechanical energy. The same transducer can also receive acoustic

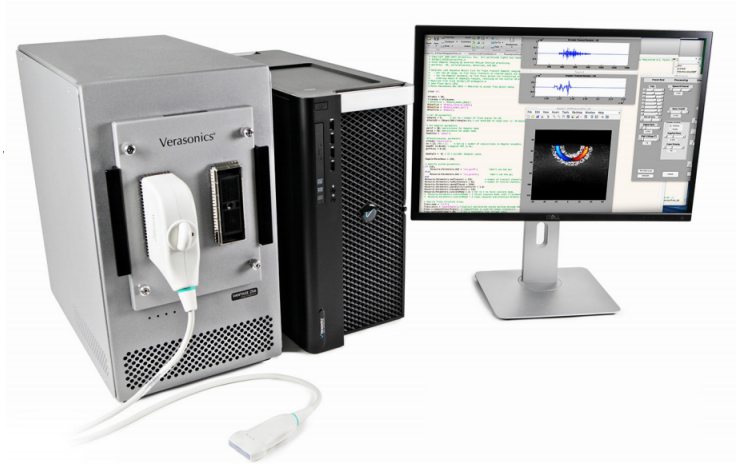

Figure 3.1: Verasonics Vantage 256 system with a probe connected

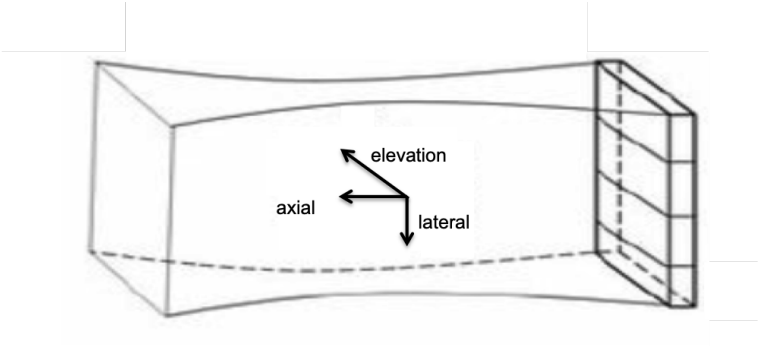

Figure 3.2: Schematic view of a transducer with four elements and the beam directions

energy and transform it into an electric current.
Most medical ultrasound machines use a probe to make a scan. Such a probe consists of many active elements, where the number of elements depends on the type of probe.
The resolution of a particular transducer can be expressed in a spatial and temporal resolution. During this project the imaged objects are not moving thus the resolution is expressed by the spatial resolution of the transducer only.
The spatial resolution, the ability to distinguish between two points at a particular depth, is determined by the lateral, axial and elevation resolution. Figure 3.2 shows the lateral, axial and elevation direction of a transducer with four elements.

The lateral resolution is the minimum distance that can be distinguished between two reflecting points located perpendicular to the ultrasound beam propagation. The lateral resolution is high when the width of the ultrasound beam is narrow. When using a multi-element transducer, grating lobes (extra beams surrounding the main beam) can be formed and possibly cause artefacts and reduce lateral resolution. Using low-frequency transducers will deteriorate the lateral resolution due to the short near-zone length of the transducer. A profound explanation of the near-zone and far-zone length of transducers can be found in [21].
The axial resolution is the minimum distance that can be differentiated between two reflecting points located parallel to the direction of the ultrasound beam. Mathematically, it is equal to half the transmitted spatial pulse length, where the spatial pulse length is the product of the wavelength and the number of cycles in a pulse. Thus when the transmitted pulse length is short the axial resolution is high. The number of cycles is determined by the damping of the piezo-electric elements after excitation. The wavelength is determined by the operating frequency of the transducer. One could argue that optimally the transducer transmits a low number of cycles at a high frequency. However, this causes problems related to attenuation. Whereas the attenuation depends on the propagation medium and the frequency. High-frequency pulses are attenuated well, which can lead to the extinction of the pulses before it is received by a transducer. Furthermore, a strong damping of the piezo-element is associated with lower signal-intensity emission. The increasing attenuation at longer depths is minimized by the amplification of signals received at later times, this is called Time Gain Control (TGC).
During this study, two types of probes are used: a P4-1 probe and an L7-4 probe. The properties of these probes will be explained.

3.2. Water-cup setup

A water-cup setup is built to obtain reflection and transmission ultrasound data. This water-cup is used to scan a phantom and an ex-vivo human breast. The phantom study gives insight into the operability of the measurement setup and the imaging algorithms.
In this study, a differentiation between reflection and transmission data is made. Reflection data is defined as the signal that is sent by one probe and received by the same probe. Whereas transmission data is sent by one probe and received by the elements of another probe. This is an effective way to split, analyze and process the two types of data. However, there are also other ways to differentiate reflection and transmission signals

from each other.

3.2.1. Setup

The water-cup setup includes a plastic cup and four P4-1 probes. A P4-1 probe is a phased array transducer transmitting frequencies from one to four megahertz. It has a linear piezo-element alignment and has a small footprint. It consists of 96 small elements. The elements can be excited independently of each other. This type of probe is for example used for brain and cardiac examinations. The specifications of the P4-1 probe are listed in Table 3.1.

Four of these probes are used to acquire reflection and transmission data. These probes are used because they can transmit relatively low frequencies. These low frequencies are necessary for Born inversion, as this is a computationally expensive algorithm. The measurements are done using a pulse with a centre frequency of 1.5 MHz. Figure 3.3 shows an example of the wavelet and the frequency spectrum of the signal that is transmitted by the P4-1 probe. It shows that the wavelet uses circa 4 cycles to build a wave with frequencies from 0.5 to 2.5 MHz. A centre frequency of circa 1.5 MHz is used, thus the width of the elements is smaller than half the wavelength. Therefore, the elements transmit in approximation cylindrical waveforms.

The Verasonics system has only two connectors, whereas the built water-cup system includes four P4-1 probes. Two probes are used at the same time for each measurement. After a measurement the probes are disconnected from the Verasonics system and another combination of probes is connected to the system. There are six combinations that can be made with the four probes, using two probes at the same time. Each measurement consists of events. During an event, one element is used as transmitter and all the elements work as a receiver. Thus, a single measurement comprises 192 events.

Table 3.1: Specifications of the P4-1 probe

$\#_{\text{elements}}$	96
element-width (mm)	0.245
element-spacing (mm)	0.295
kerf (mm)	0.05
elevation height (mm)	16
elevation focus (mm)	80

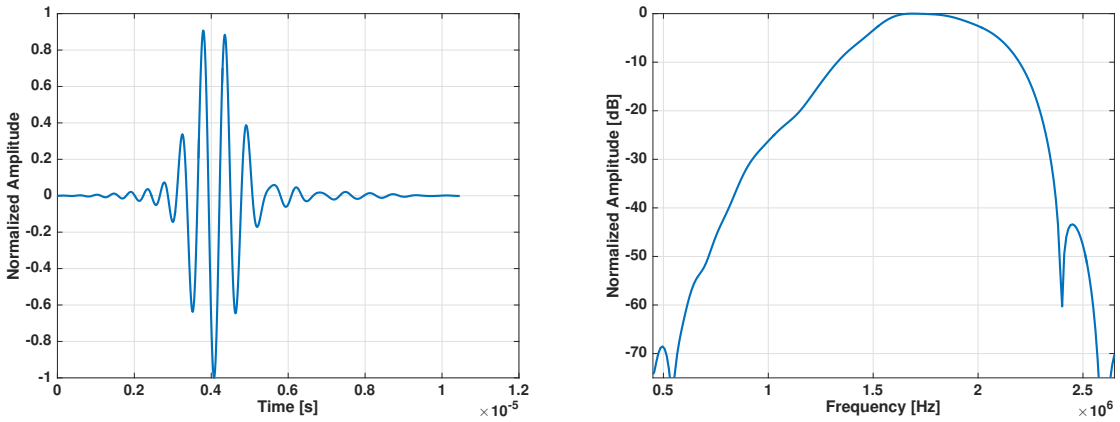

(a) Transmitted wavelet of P4-1 probe

(b) Transmitted frequency spectrum of P4-1 probe

Figure 3.3: Example of the transmitted field of the P4-1 probe with a frequency bandwidth centred around 1.5 MHz

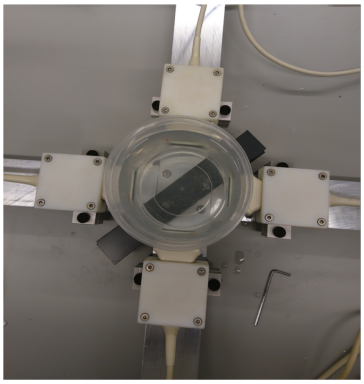

(a) Empty water-cup setup

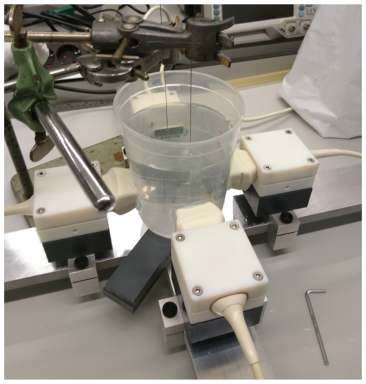

(b) Water-cup with 2 wires to calibrate probe positions

Figure 3.4: The water-cup setup that is built to obtain reflection and transmission data.

Figure 3.4 shows the water-cup setup. The wires in Figure 3.4 (b) are used to calibrate the probe positions. First, a manual measurement is made to obtain the probe coordinates, using the direct travel time between two facing probes through the with water filled cup. Next, a separate SAFT image is made from the wires for each probe. Afterwards, the probe coordinates are adapted so that the wires in the SAFT images perfectly overlay each-other.

3.2.2. Imaging and Inversion

One imaging algorithm, i.e. SAFT, and two types of inversion algorithms, i.e. ART and BI are used. The SAFT, ART and BI algorithms are written in MATLAB. These algorithms are used to image a phantom. The phantom is made from agar and includes a plastic straw and two copper wires. Figure 3.5 shows the water-cup with the phantom. This type of phantom is used because it was used with the two-transducer circular DBUS setup. This is useful for a possible comparison of the obtained images of the two measurement systems.

The size of the phantom in the x-y-z-dimensions is respectively 2.3×0.5×15 cm. The speed of sound of the agar is obtained by comparing the direct transmission travel-time of an empty measurement with that of a

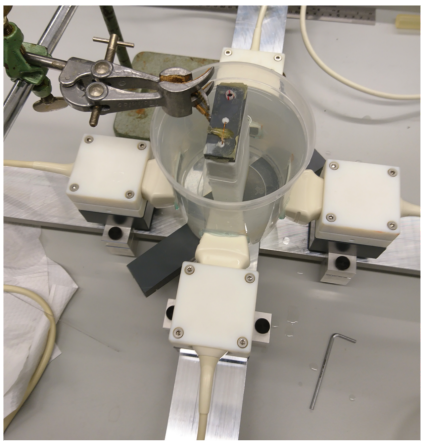

(a) Water-cup with phantom

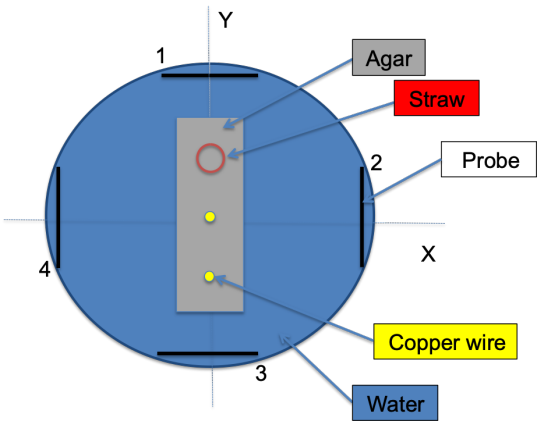

(b) Sketch of the water-cup setup with phantom

Figure 3.5: The water-cup setup including the agar phantom

phantom measurement. Thus the travel-time of a ray travelling through only water and one travelling through the water and the agar is determined. Combining this with the dimensions of the agar phantom, a speed of sound of approximately 1492 m/s is found for the agar. This is different from the literature value for the speed of sound of 1540 m/s for agar [22]. This is probably due to the difference in fabrication and conservation of the agar. The phantom includes also two copper wires with a speed of sound of circa 4600 m/s. And a plastic straw. The type of plastic is undetermined, but most straws are made of polypropylene. Polypropylene has a speed of sound of circa 2300 m/s[23].

Processing the data, 96 out of 384 available transducers are selected as a source and all 384 transducers are used as a receiver for each source. This is done following Ramirez & van Dongen [24]. They showed that for reducing the amount of analyzed data, it is better to reduce the number of sources compared to the number of receivers when using non-linear inversion algorithms. In this study, only linear imaging and inversion algorithms are used, however for possible comparison of these results with the results of non-linear inversion algorithms this configuration is chosen.

Born Inversion

The Born inversion algorithm employs the incident field $\hat{p}^{inc}(\vec{r}')$ to construct an image, as showed in equation (2.17). The incident field $\hat{p}^{inc}(\vec{r})$ can be expressed as

$$\hat{p}^{inc}(\vec{r},\omega) = i\omega\rho_0 \int_{\vec{r}'\in D} \hat{G}\left(\vec{r}-\vec{r}',\omega\right)\hat{q}\left(\vec{r}',\omega\right) dV\left(\vec{r}'\right). \tag{2.12}$$

To obtain $\hat{p}^{inc}(\vec{r},\omega)$, we assume that the source-term $\hat{q}\left(\vec{r}',\omega\right)$ acts as a point-source. Then, it can be expressed by

$$\hat{q}\left(\vec{r},\omega\right) = \hat{\mathrm{w}}(\omega)\delta\left(\vec{r}-\vec{r}'\right). \tag{3.1}$$

Combining (2.12) and (3.1), we get

$$\hat{p}^{inc}(\vec{r},\omega) = i\omega\rho_0\hat{G}\left(\vec{r}-\vec{r}',\omega\right)\hat{\mathrm{w}}(\omega). \tag{3.2}$$

To obtain $\hat{p}^{inc}(\vec{r},\omega)$ for the water-cup setup, two probes are facing each other with water in between. The middle element of the first probe is used as source and the middle element of the second probe is used as receiver. Consequently equation (3.2) can be written as

$$\hat{p}^{inc}(\vec{r}^R,\omega) = i\omega\rho_0\hat{G}\left(\vec{r}^R-\vec{r}^S,\omega\right)\hat{\mathrm{w}}(\omega) = \mathrm{A}\hat{\mathrm{w}}(\omega) \tag{3.3}$$

where $\mathrm{A} = i\omega\rho_0\hat{G}\left(\vec{r}^R-\vec{r}^S,\omega\right)$.

Now we find an expression for $\hat{\mathrm{w}}(\omega)$;

$$\hat{\mathrm{w}}(\omega) = \frac{\mathrm{A}^*\hat{p}^{inc}(\vec{r}^R,\omega)}{\mathrm{A}^*\mathrm{A}+\epsilon} \tag{3.4}$$

where equation (3.3) is multiplied with A^*, where the asterisk denotes the complex conjugate. Furthermore, the ϵ-term is added to stabilize the division.
For each element this signal is scaled by its relative sensitivity. The sensitivity of each element is obtained by computing the maximum absolute value of the A-scan that is sent and received by the same element and perpendicularly reflected from the flat surface of a glass cylinder.

Scaling reflection and transmission data

The Born inversion algorithm is used to reconstruct a contrast map and a speed of sound map in one image. Usually, a contrast image is acquired with reflection data. And a speed of sound map is obtained using transmission data. The water-cup gives the possibility to focus on the difference between reflection and transmission data.

The results of the circular DBUS setup show that by applying a back-propagation technique on reflection

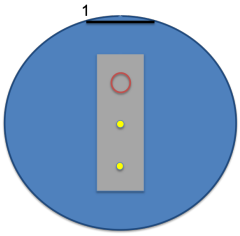

(a) Schematic setup of water-cup with one probe

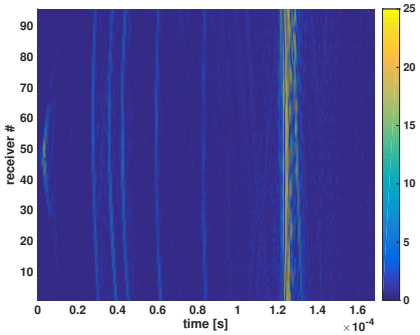

(b) Reflection data b-scan of straw-wire phantom

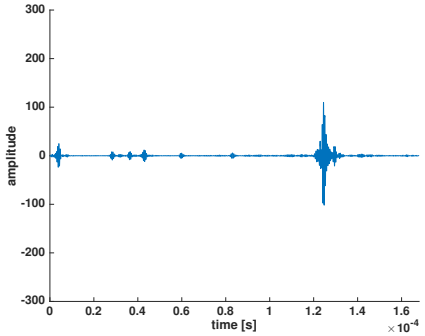

(c) Reflection data a-scan of straw-wire phantom

Figure 3.6: Example of reflection data of a straw-wire phantom measurement

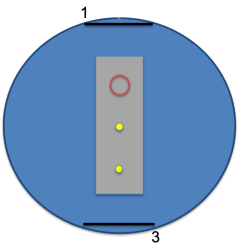

(a) Schematic setup of water-cup with two probes

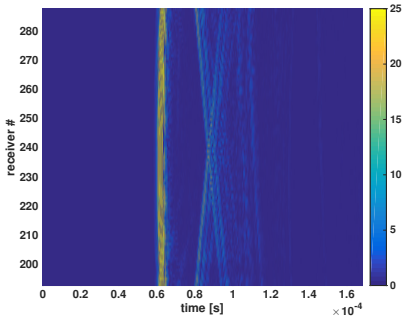

(b) Transmission data b-scan of straw-wire phantom

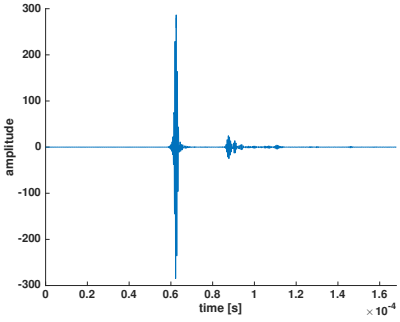

(c) Transmission data a-scan of straw-wire phantom

Figure 3.7: Example of transmission data of a straw-wire phantom measurement

and transmission data, the image is particularly built by transmission signal. The amplitude of transmission data is, depending on the heterogeneity of the measured object, significantly higher than that of the reflection data. The measurements of the build water-cup setup, see Figure 3.6 and 3.7, demonstrate this too.
Figure 3.6 shows the raw reflection data for the measurement setup with one probe, Figure 3.6(a). Figure (b) is a B-scan, where the middle element of probe 1 is used and all 96 elements are used as a receiver. The reflections of the agar, straw and wires can be found between 0.02 ms and 0.1 ms. Whereas the reflection around 0.125 ms is from the other side of the cup. The signal before 0.1 ms is the signal that is received directly after transmitting.
Figure 3.7 shows transmission data of the probe acquisition setup shown in Figure 3.7 (a). In Figures 3.7 (b) and (c) around 0.06 ms the transmission signal that has travelled through water and the phantom can be seen. The signal between 0.08 and 0.1 ms is from the sides of the cup.

The difference in the amplitude between reflection and transmission signal for this straw-wire-agar phantom can be seen by comparing Figure 3.6 and 3.7. This knowledge can be used to scale the transmission and reflection data. The scaling is carried out by adding a parameter λ to the Born inversion algorithm. This λ is obtained by dividing the maximum absolute amplitude of a direct transmission signal by the maximum absolute amplitude of the reflections of the phantom. In the Born inversion scheme Table 2.1, the scattered field $\hat{p}^{sct}(\vec{r},\omega)$ for reflection data and the source term $\hat{q}\left(\vec{r}',\omega\right)$ for the reflection data will be scaled with the obtained λ factor.

Source-receiver frequency picking for BI
Born inversion is an iterative inversion method. The algorithm analyses for each iteration the signal of the selected sources, receivers and frequencies. Compared to SAFT, the computational load for BI is significantly higher. Therefore, in applying for example Born inversion, it is common to pick only a few frequencies from the lower part of the frequency bandwidth. The frequencies are picked from the lower part of the spectrum for convergence reasons [25].

A method is proposed that evaluates randomly picked frequencies for each reflection data based source-receiver combination. In this way, all frequencies of the transmitted signal will be taken into account, while the computing time will not be affected.
For each of the four probes 24 sources and 96 receivers are used to acquire reflection data. Thus, in total 24×96×4=9216 source-receiver combinations can be made. Each source-receiver combination will use 10 randomly picked frequencies, out of the 180 frequencies of the transmitted frequency spectrum, to reconstruct a contrast-map. This results in a circa 18 times faster reconstruction of the image compared to when 180 frequencies are analysed for each source-receiver combination.

3.3. Ex-vivo human breast measurement

In addition to the water-cup measurements, an ex-vivo human breast pulse-echo-scan is made. The ultrasound pulse-echo-scan will be compared with a photo of the cross-section of the breast. This is done to obtain more knowledge about the structures within the human breast and see how these structures are expressed in ultrasound images. A L7-4 probe is used to make the pulse-echo-scan.

3.3.1. Setup

The L7-4 probe is a linear array transducer. It has a linear piezoelectric crystal alignment containing 128 elements, a wide aperture and it operates at frequencies in the range of 4 to 7 MHz. The piezoelectric elements are relatively wide therefore they are able to transmit in approximation a plane wave. The linear probe is used for applications such as vascular examination and thyroid examination. Table 3.2 shows the specifications of the L7-4 probe.

A single L7-4 probe is used to obtain pulse-echo data of an ex-vivo human breast. This probe is used because it can transmit relatively low frequencies. This can be useful for generating a model of the measured breast, what is done by Govers and Scherders [18, 26]. Also, the focus distance and the elevation height of the L7-4 probe, shown in Figure 3.8, are sufficient for scanning the heterogeneous breast. The width of the focused beam is calculated with

$$\text{Width of focused beam} \approx \frac{\text{focal length} \times \text{wavelength}}{\text{aperture}}. \tag{3.5}$$

The transmitted wavelength, at 5.2 MHz and a background speed of sound of approximately 1500 m/s, is ~0.3 mm. Thus the wavelength is in the same range as the width of the elements. This causes grating lobes

Table 3.2: Specifications of the L7-4 probe

$\#_{\text{elements}}$	128
element-width (mm)	0.250
element-spacing (mm)	0.298
kerf (mm)	0.048
elevation height (mm)	7.5
elevation focus (mm)	25

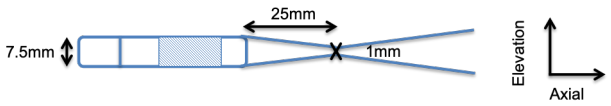

Figure 3.8: Schematic view of the elevation resolution of a L7-4 probe

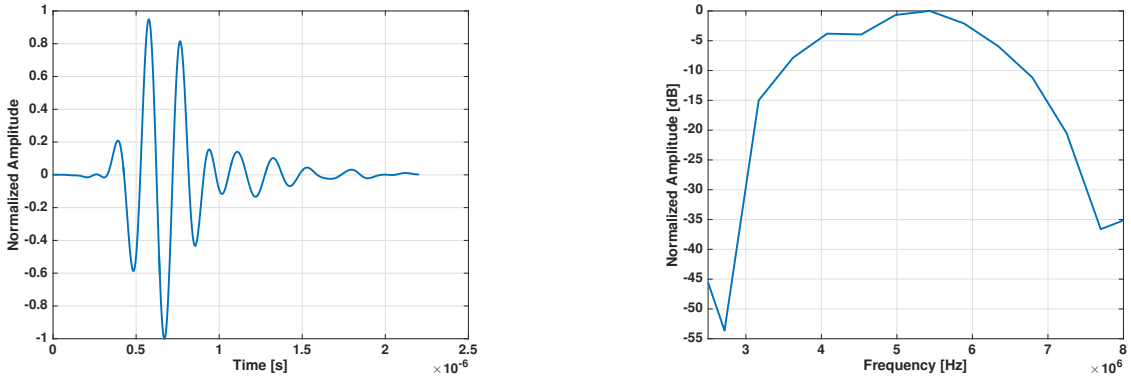

(a) Transmitted wavelet of L7-4 probe

(b) Transmitted frequency spectrum of L7-4 probe

Figure 3.9: Example of the transmitted field with a frequency spectrum from 4 to 7 MHz centered around 5.2 MHz

to occur. An angle-dependent taper is used to filter out the artefacts caused by the grating lobes. Figure 3.9 includes the wavelet and the frequency spectrum that is transmitted by the L7-4 probe. The wavelet consists of circa three cycles to form a wave from 4 to 7 MHz, centred around 5.2 MHz.

3.3.2. Method

The ex-vivo breast measurements are performed at the Pathology Department of the Erasmus MC. Following the protocol five measurements could be done [18, 26]. The ablation mammas available at the Pathology differ much in size and amount of skin. Also, some breasts are preventively removed and others have a tumour inside. The amount of skin on the ablation mamma depends on the type of breast-reconstruction that is performed after the surgery.

To make a proper scan of the ex-vivo human breast, the probe needs to be positioned correctly. The optimal position is the place where different types of tissue, such as skin, fat, tumour, cysts and glandular tissue, can be distinguished. This location is determined by first making a real-time pulse-echo-scan. The real-time scan is made by exciting each of the 128 elements one by one and use all 128 elements as receiver. After the right location is determined, a high-precision scan is made. The high-precision scan is made by exciting each of the 128 elements 32 times and receiving with all 128 transducers. In this way, the signal can be averaged 32 times. This will increase the signal-to-noise ratio, when random noise is present.

Figure 3.10 shows the procedure that is executed at the pathology department of the Erasmus MC. The characteristics of the patient and the breast are listed in Table 3.3.

Table 3.3: Patient characteristics

Age	45
Menopausal state	pre-menopausal
Cup-size	C
Weight breast	657g
Reason for ablatio	preventive: BRCA 1 gene mutation

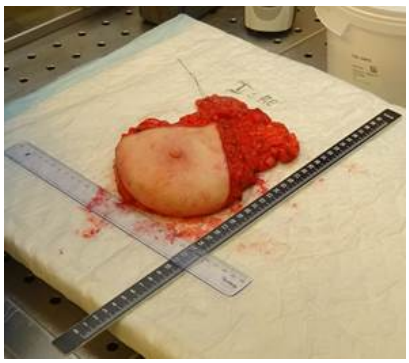

(a) An ablation mamma. The size of the breast is measured when it arrives at the pathology department.

(b) The mamma is dyed to mark its orientation. The paint is dried so it won't leak onto other sides.

(c) The mamma is pinned on a plastic covered carton plate to minimize the movement during the measurement

(d) A real-time scan is made to find different structures in the breast. After the real-time scan the probe is set in a tripod and a high-precision scan is made

(e) At the place where the scan is made a thread is spanned and pinned on the carton plate. This thread works as an alignment for the knife.

(f) The mamma is cut at the desired location to obtain a cross-section of the mamma. A photo of the cross-section is taken and now we are able to compare an ultrasound scan with a cross-sectional photo

Figure 3.10: Example of the procedure at the pathology to obtain a cross-sectional photograph of the mamma at the location where the ultrasound scan is made

4

Results and discussion

In this chapter, the results of the water-cup setup and the ablation mamma are shown. For the water-cup measurement, the results for scaling the reflection data with the transmission data and picking random frequencies for reflection data using Born inversion are shown. Also, the images obtained using different reconstruction algorithms are shown and compared. Furthermore, the ultrasound pulse-echo image of the ablation mamma is compared with the photograph of the cross-section. In the end, the SAFT image of an ex-vivo human breast scanned with the four-probes water-cup setup is shown.

4.1. Straw-wire phantom measurement

To make a fair comparison between various imaging algorithms, it is tried to execute the same data processing. Table 4.1 shows the configurations that are used to reconstruct the images. Figure 4.1 shows a sketch of the water-cup with the phantom inside.
The temperature of the water was 21.7 °C before the measurement and 21.5 °C after the measurement. This results in a speed of sound of circa 1487 m/s of the water. The speed of sound is calculated with a fifth order polynomial proposed by W. Marczak [27].

4.1.1. Born Inversion

Source-receiver frequency picking for reflection data

It is common to use a few frequencies from the lower part of the frequency spectrum to reconstruct a speed of sound map with a Born inversion algorithm. Figure 4.2 shows, for the straw-wire phantom, the difference between images solely based on reflection data and images solely based on transmission data. The difference between Figures 4.2 (a),(c) and (d) shows that a back-propagation algorithm is not able to reconstruct a correct contrast image from the reflection signal with only a few frequencies from the lower or the higher

Table 4.1: Image configurations

$\#_{src}$	96
$\#_{rcv}$ per source	384
f_c	1.5 MHz
dx	0.1475 mm
dimensions	7 cm x 7 cm
c_0	1485 m/s

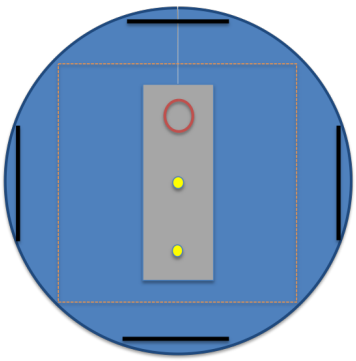

Figure 4.1: Schematic overview of the water-cup setup with the phantom

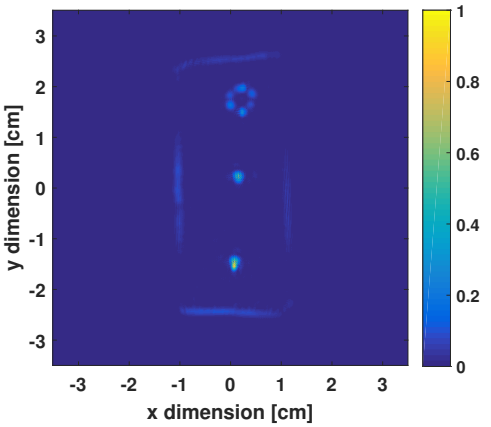

(a) Only reflection signal and all 180 frequencies from 0.6 to 2.39 MHz of the transmitted signal are used to construct the image

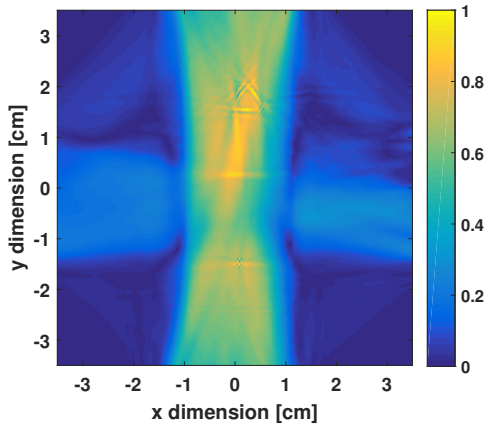

(b) Only transmission signal and all 180 frequencies from 0.6 to 2.39 MHz of the transmitted signal are used to construct the image

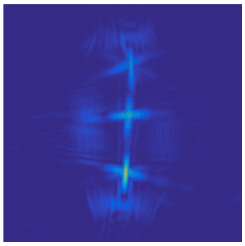

(c) Only reflection signal and only 10 frequencies, between 1.06-1.16 MHz, of lower part of transmitted signal

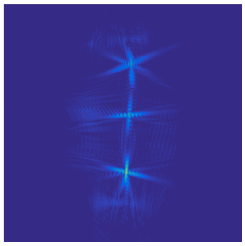

(d) Only reflection signal and only 10 frequencies, between 2.2-2.3 MHz, of higher part of transmitted signal

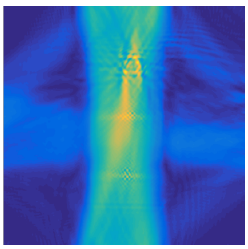

(e) Only transmission signal and only 10 frequencies, between 1.06-1.16 MHz, of lower part of transmitted signal

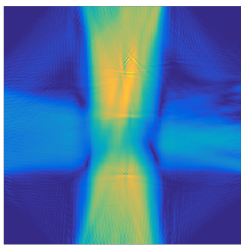

(f) Only transmission signal and only 10 frequencies, between 2.2-2.3 MHz, of higher part of transmitted signal

Figure 4.2: Example of difference between reflection and transmission data back-propagation images. The lower figures show the images where only a small part of the transmitted frequency bandwidth is used to construct an image.

part of the frequency bandwidth. Whereas Figures 4.2 (b),(e) and (f) show that the transmission signal images do not differ that much from each other, when using less frequencies. This suggests that for reconstructing a contrast image with reflection data it is necessary to analyze all frequencies of the transmitted frequency spectrum.

Now focusing on reflection data. Figure 4.3 shows three contrast images. Image (a) is reconstructed using all 180 frequencies, image (b) is reconstructed using 10 out of 180 frequencies from 1.3 to 1.4 MHz and image (c) is reconstructed using 10 frequencies for each source-receiver combination picked randomly out of the 180 frequencies. The images at the top in Figure 4.3 are produced with different frequency configurations. The bottom images show the frequency combinations that are used to reconstruct the top images.
For reflection data, it is not possible to reconstruct a contrast image when only a few frequencies from the lower part of the spectrum are taken. All frequencies of the transmitted wave are needed to reconstruct a proper contrast image. When analyzing all frequencies the computing time will be high.
Figure 4.3 (c) shows the results of the random frequency picking. This method is able to find the contrasts at the correct locations within the Born approximation. The reconstruction time is 18 times faster but the signal-to-noise ratio is decreased. The speckle pattern of the agar is lost in the noise caused by the aliasing. This is not a problem when a speed-of-sound map is reconstructed. The different tissues can than be distinguished by their difference in speed of sound.

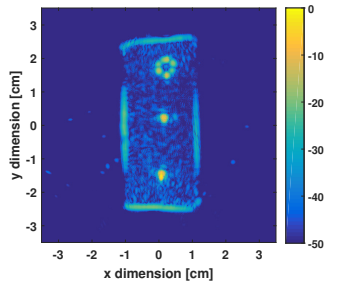

(a) Back-propagation image of phantom with all 180 frequencies from 0.6 to 2.49 MHz of the reflection data used to reconstruct image

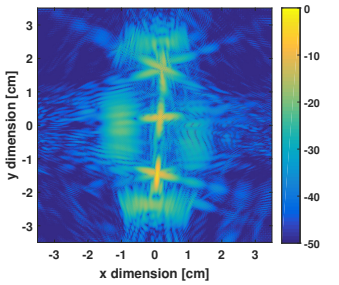

(b) Back-propagation image of phantom with 10 frequencies from 1.3 to 1.4 MHz of the reflection data used for each source-receiver combination to reconstruct image

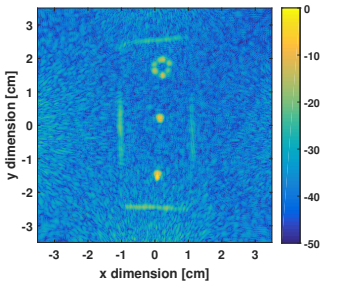

(c) Back-propagation image of phantom with 10 random frequencies in the range of 0.6 to 2.49 MHz of the reflection data used for each different source-receiver combination

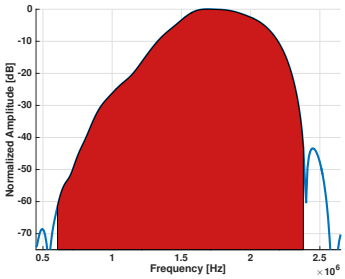

(d) The frequencies that are used to reconstruct reflection image (a); all source-receiver combinations use all 180 frequencies in the range from 0.6 to 2.39 MHz

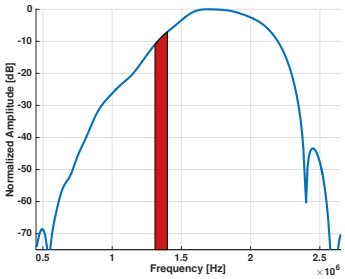

(e) The frequencies that are used to reconstruct reflection image (b); all source-receiver combinations use all 10 frequencies in the range from 1.3 to 1.4 MHz

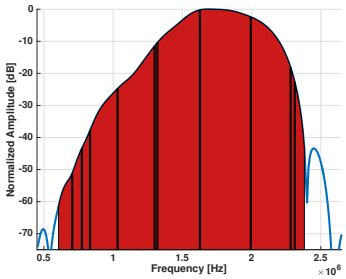

(f) The black lines show the frequencies that are randomly picked for one source-receiver combination, the red color indicates the frequencies for all source-receiver combinations; each source-receiver combination uses 10 random frequencies in the range from 0.6 to 2.39 MHz to reconstruct image (c)

Figure 4.3: Reflection data back-propagation images of the straw-wire phantom with various frequencies for source-receiver combinations

Scaling of reflection data with transmission data for BI

Figure 4.4 shows two BI images (after eight iterations) that are reconstructed using reflection and transmission data. Both images are made with 10 frequencies in the range from 1.3 to 1.4 MHz. In Figure 4.4 (b), the reflection data is scaled with the transmission data by a factor $\lambda = 24.4$.

The reflection data is now primarily used to reconstruct the contrasts. Whereas the transmission data is still able to produce a speed of sound map. The contrasts are not correctly imaged because only 10 out of 180 frequencies are used. Also, image (b), in which the reflection data is scaled, looks smoother than image (a). The reflection data seems to smooth out the artefacts caused by the transmission data.

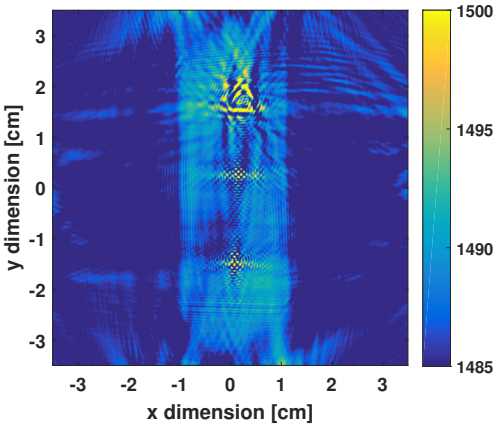

(a) Born inversion image of phantom with 10 frequencies in the range from 1.3 to 1.4 MHz of the reflection and transmission data used to reconstruct image

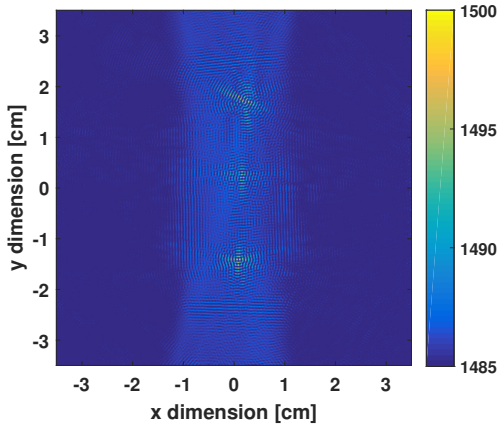

(b) Same configuration of sources, receivers and frequencies is used to reconstruct image as in image (a) but the reflection data is scaled with the amplitude of the transmission data

Figure 4.4: Born inversion images of the straw-wire phantom; in image (b) the reflection data is scaled with the amplitude of the transmission data

Source-receiver frequency picking for reflection data and scaling of reflection data with transmission data for BI

Figure 4.5 (b) shows the image where the reflection data is scaled by λ=24.4 and the frequencies are picked randomly for reflection data. This image is compared with Figure 4.5 (a), that is reconstructed in the old manner.

The contrasts are better shown in Figure 4.5 (b). The artefacts caused by the transmission signal are not there anymore. However, the noise caused by aliasing from the reflection data smoothens the image. This disturbs the reconstruction of a speed-of-sound profile. The aliasing noise should be filtered out before a speed of sound profile is made.

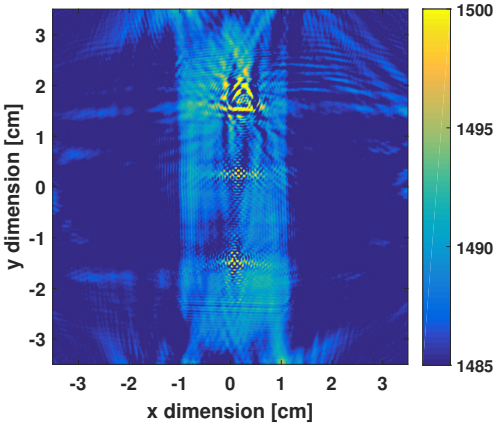

(a) Born inversion image of phantom with 10 frequencies from 1.3 to 1.4 MHz of the reflection and transmission data used to reconstruct image

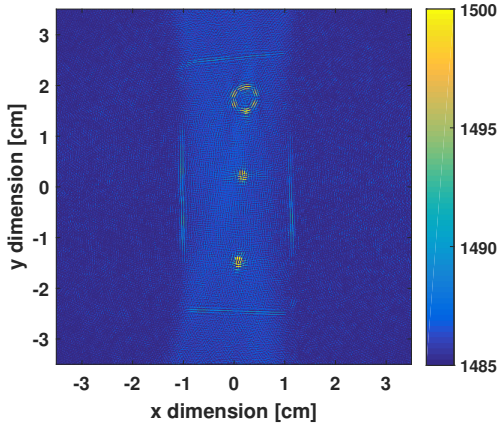

(b) Same configuration is used to reconstruct image as in image (a) but the reflection data is scaled with the transmission data and for the reflection data there are for each source-receiver combination 10 frequencies randomly picked in the range of 0.6 to 2.49 MHz

Figure 4.5: Born inversion images of the straw-wire phantom; in image (b) the reflection data is scaled with the transmission data and for the reflection data 10 frequencies are randomly chosen for each source-receiver combination

4.1.2. comparison of SAFT, ART and BI

Figure 4.6 shows the resulting SAFT, ART and BI images for reflection and transmission data. Whereas SAFT only uses reflection data to reconstruct a contrast image and ART only works with transmission data to compute a speed of sound map.

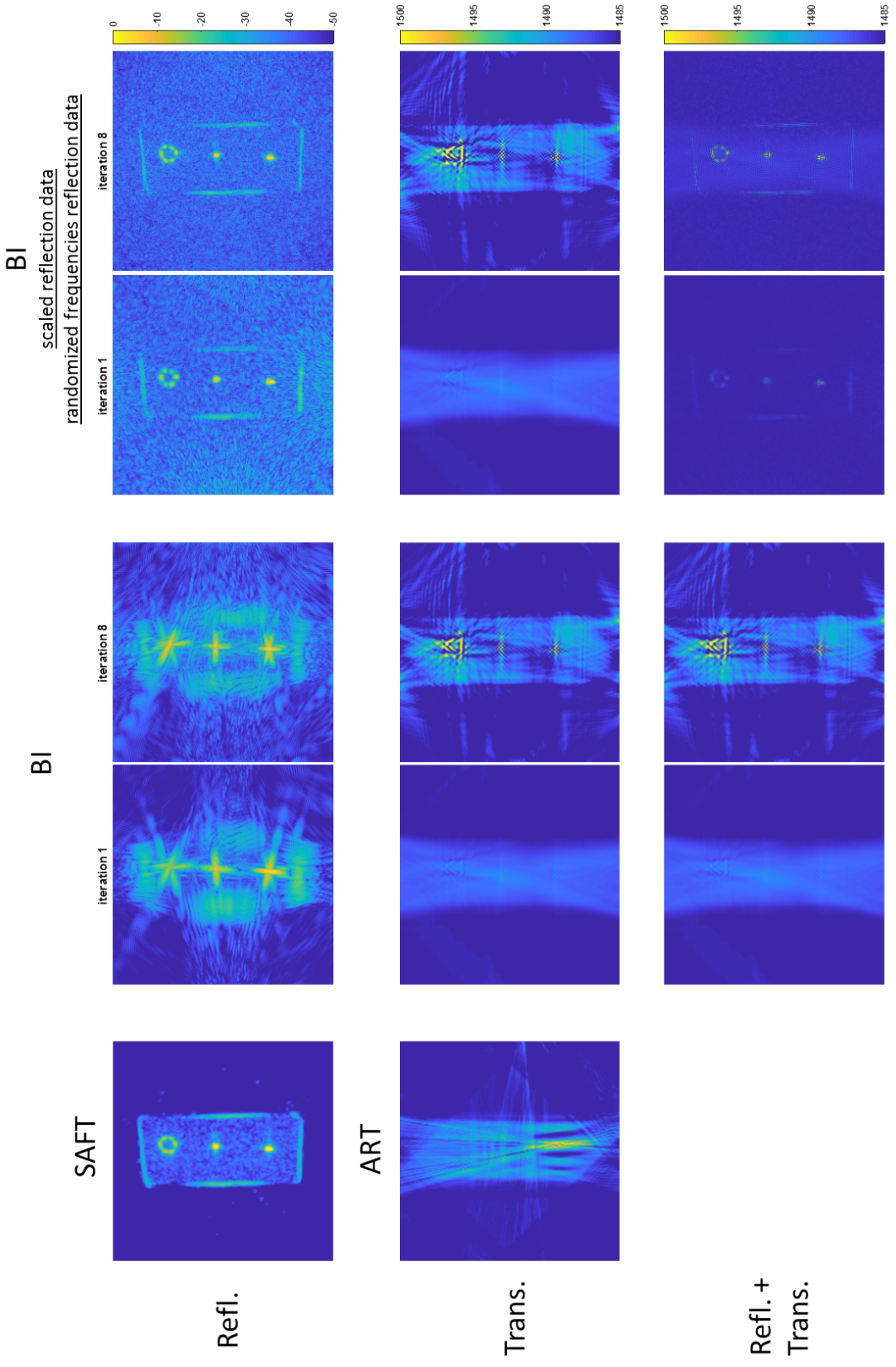

Figure 4.6: Comparison of SAFT, ART and BI images for reflection, transmission and reflection plus transmission data

The SAFT image shows the agar phantom with the straw and two wires nicely. The speckle inside the phantom is due to the tissue mimicking properties of the agar. The speckle is caused by the scattering of the ultrasound from the structures in the agar. The size of the phantom in the vertical direction is bigger than the size of the P4-1 probe. Due to the gaps in the measurement-setup, the reflections from the parts of the phantom that are not in front of a probe are not received. The straw is not a closed circle; it is rather a circle built by dots. The dots are reconstructed by the reflections from the straw received by each probe. Appendix B shows the SAFT images for different probe combinations.

The images in the middle column are reconstructed using Born inversion and are made using 10 frequencies in the range of 1.3 to 1.4 MHz, whereas the transmitted signal covers the range from 0.6 to 2.39 MHz. Figure 4.3 (e) shows the picked frequencies in the available frequency spectrum. The first iteration BI contrast image with only reflection data shows that picking 10 out of 180 frequencies is not sufficient to reconstruct a proper contrast image of the straw-wire phantom. The BI algorithm does not have enough data to place the contrasts at the correct position.
The eighth iteration, reflection data based BI image shows that the BI algorithm tries to sharpen the contrasts. However, it is still not able to find the correct shape of the objects in the phantom. Also, more artefacts appear in the water.

The images in the right column are reconstructed using a Born inversion algorithm in which the reflection data is scaled with the transmission data and for each reflection data based source-receiver combination 10 random frequencies are analyzed.
The first iteration BI image shows the contrasts of the phantom, but noise is present in the image. The speckle pattern of the agar is lost in the noise. The contrasts have a resolution similar to the contrasts present in the SAFT image. This is expected, as the first iteration of BI with reflection data is similar to SAFT in the frequency domain.
The eighth iteration BI image shows that the contrasts are sharper than the contrasts present in the first iteration BI image. The noise pattern is also different from the noise in the first iteration BI image, it seems that the speckle-noise also gets sharpened.

For the reflection data images, the SAFT image is the only image that shows the speckle-pattern for the tissue-like agar. The Born inversion algorithm for which 10 frequencies are picked from the lower-part of the transmitted frequency spectrum is not able to reconstruct a proper contrast image. The eight iteration BI image, where the reflection data is scaled and random frequencies are picked for reflection data source-receiver combinations, shows the sharpest contrasts. However, the speckle pattern of the tissue-like phantom is lost in the noise.

In the ART transmission image, it can be seen that ART is a ray-based method, the rays are projected on the imaging domain. The ART algorithm is not able to locate the straw and the two wires. And the top and bottom of the phantom in the vertical direction are not clearly visible. This is because the directions of the rays passing those areas have almost the same orientation. Furthermore, a fan-beam geometry starting at the second probe can be spotted. This structure may be caused by a broken element. A speed of sound of circa 1495 m/s is found for the agar. The ART image is made by T. Bouchan.
Figure 4.7 shows the ray-density distribution of the water-cup setup. It shows that there are spots in the imaging domain that are not crossed by rays. This can lead to artefacts in the image when a bigger phantom is imaged. The straw-wire phantom that is used in this study lays in the horizontal direction within the blank spots. The rays are unevenly distributed because of the gaps in the setup. In the areas between two probes, there are only rays travelling between the two probes. E.g. in the area between probe 1 and probe 2, rays are only travelling from probe 1 to probe 2 and vice versa.

The first iteration transmission data based BI image shows a speed of sound map with a rectangular shape in the middle. This is a vertically smeared out agar phantom. The top and bottom of the phantom cannot be distinguished, this is similar to ART. However, in this case, the amplitude of the waves travelling from the lower and top probes to the side probes have a smaller amplitude than the waves travelling straight forward. The straw and two wires appear vaguely in the image.
In the eighth iteration transmission data BI image, the straw and two wires can be seen. However, the straw has a somewhat triangular shape. This shape is due to the reflections of the straw obtained by various probe

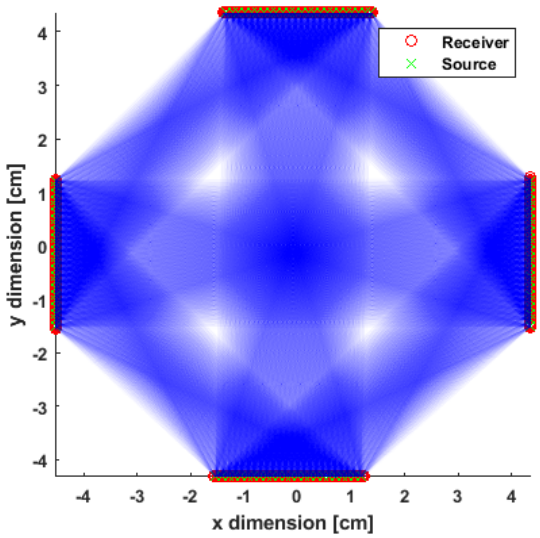

Figure 4.7: The ray-density distribution in the water-cup setup

combinations. The upper and lower boundaries of the phantom are not clearly visible. Furthermore, some artefacts appear in the water. These artefacts may be caused by the imperfect estimation of the incident field. The wires are built by a dotted pattern. This pattern may be due to the born approximation, where a constant background speed of sound is taken. This is not realistic and can result in various allocations of the same contrast by different probes, as the travel time of the sound wave for a particular distance depends on the media through which it travels.

For the transmission data images, clear differences can be spotted between the ray-based and wave-based reconstruction methods. ART is not capable of finding the straw and two wires, whereas the BI images show them. Both algorithms can obtain a speed of sound map of the agar. However, there appear artefacts in both images. The artefacts at the top and bottom of the phantom can be explained by the gaps between the probes in the measurement setup. Furthermore, artefacts in the BI images can be caused by the imperfect estimation of the incident field.

The middle column BI images for reflection + transmission data are dominated by the transmission data. This is because the amplitude of transmission data is higher than the amplitude of the reflection data when using a signal with a centre frequency of 1.5 MHz to measure this phantom.

In the right column, the first iteration BI image for reflection + transmission data shows a speed of sound map in which only the contrasts can be distinguished from the water. In the eighth iteration BI image, the contrast of the agar phantom are nicely visible and the speed of sound difference between the agar and water is found. The agar has a homogeneous speed of sound of approximately 1488 m/s.

The built water-cup is not able to construct a proper speed of sound map of the agar phantom. This is due to the gaps between the probes. From a theoretical point of view, this can be explained partly by the Kirchhoff Integral

$$\hat{p}(\vec{r}_A) = -\oint_S \left(\hat{p}\nabla\hat{G} - \hat{G}\nabla\hat{p}\right)\cdot\vec{\mathrm{n}}\,dS. \tag{4.1}$$

It states that the sound pressure at a point A in space can be calculated when the pressure $\hat{p}$ and the gradient of the pressure (velocity) $\nabla\hat{p}$ are known on a closed surface S around a point A. For the built water-cup, the pressure cannot be measured at the gaps between the probes, this makes it harder to determine the pressure at the points between the probes.

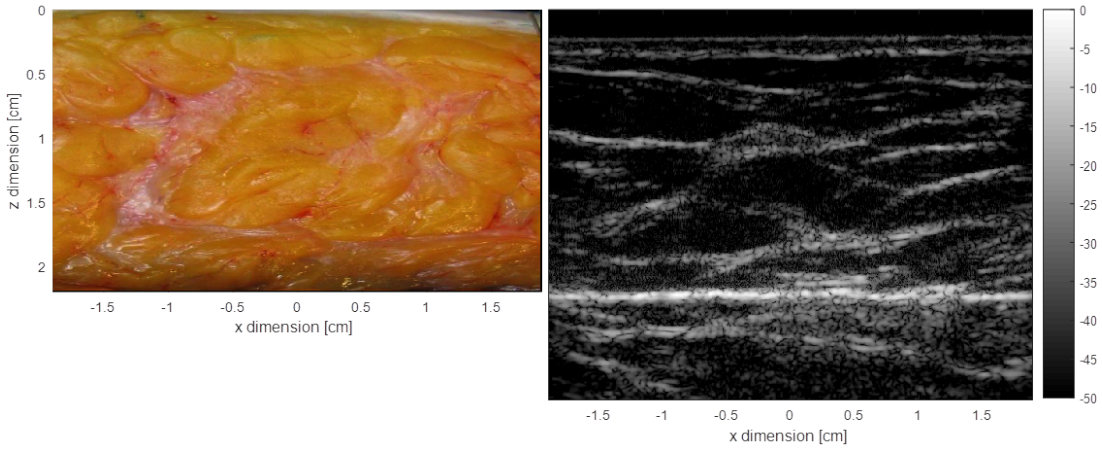

Figure 4.8: Images of the ablatio mamma; left is the cross-sectional photograph of the scanned tissue, right is the SAFT image of the pulse-echo-scan

4.2. Ex-vivo human breast measurement

4.2.1. Comparison of a cross-sectional photograph of a breast with its pulse-echo-scan

Figure 4.8 shows two images of an ablation mamma obtained at the pathology department of the Erasmus MC. Image (a) shows a cross-sectional photograph of the mamma, the cross-section is made at the place of the pulse-echo-scan. Image (b) shows the SAFT image of the pulse-echo-scan.

In image (a) the different types of tissue can be roughly distinguished by their colour. Yellow/orange is fatty tissue, the white colour within the fatty tissue indicates glandular tissue, the white in the right top corner is skin and the red colour is blood.
In image (b) the black colour indicates a homogeneous medium. The speckle pattern or white colour indicates a contrast. Therefore the fatty tissue is represented by the dark areas. Whereas the glandular tissue is shown as white colour or speckle pattern. The glandular tissue induces a speckle pattern, the sound waves scatter from the small structures in the glandular tissue. The white lines can also indicate a transition from one fatty structure to another fatty structure. The horizontal, bright white line at 2.2 cm is the reflection from the table on which the breast lays. Below the white line of the reflection of the table, multiple scattering can be recognized. As the table works as a kind of mirror.
The structures recognized in image (a) are not found in image (b). There are several reasons for this. The main reason is the pudding-like structure of the breast. Therefore it is hard to make the cross-section at the same location as where the pulse-echo-scan is made. When the breast is cut at the position where the probe was, the breast is pressed on the table. The pressure makes the glandular tissue and fat structures shift. Another limitation is the elevation resolution of the L7-4 probe together with the heterogeneous spreading of the glandular tissue. The elevation resolution of the L7-4 probe is not high enough to detect these fine structures in the breast. Besides the speckle pattern in the SAFT image, only horizontal structures are shown. This makes it also harder to compare both images.

4.2.2. Water-cup SAFT image of an ablation mamma

In addition to the agar phantom, the 'water-cup' setup is also used to measure an ex-vivo breast of a 30 years old woman. The breast was kept on formalin during one night. This changes the tissue parameters of a breast. The breast seemed to be stiffer and the colour of the breast changed from red to grey. Figure 4.9 shows the water-cup setup with the breast inside and the SAFT image that is obtained.

In Figure (b) the white circle in the four corners comes from the reflections from the cup. The white color spots are reflections from the breast. Where the black areas are water. The breast can thus be distinguished more or less from the water. However, the structures inside the breast are not distinguishable. This is mainly due to the resolution of the P4-1 probe in the elevation direction. Figure 4.10 shows the resolution of the P4-1

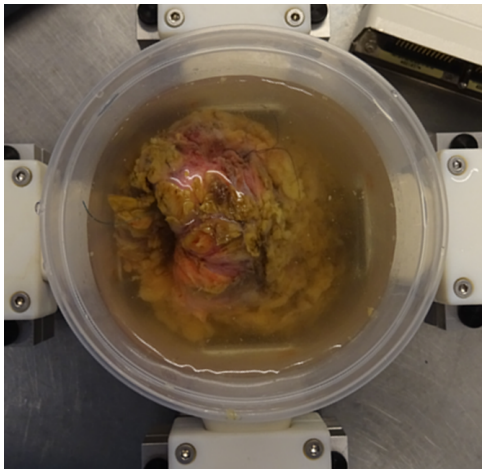

(a) Photograph of the water-cup setup with an ablatio mamma inside

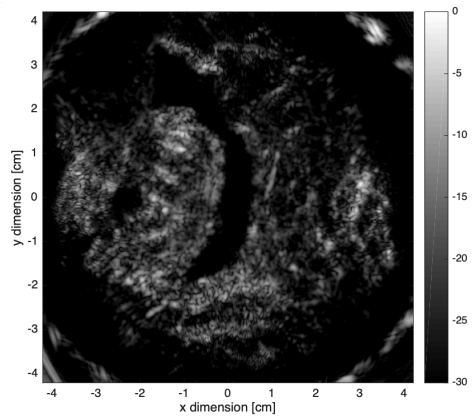

(b) SAFT image of the ablatio mamma

Figure 4.9: The water-cup measurement setup used to image an ex-vivo human breast

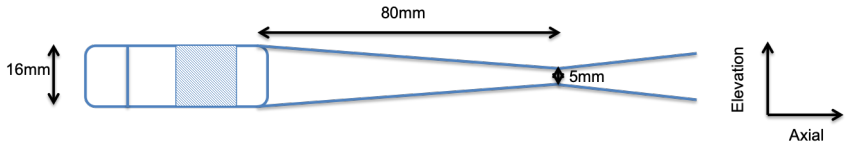

Figure 4.10: Schematic view of the elevation resolution of a P4-1 probe

probe in the elevation direction. The focus point lays at 80 mm and the resolution of the focused beam is 5 mm. The width of the focused beam is calculated with equation (3.5).

5

Conclusion and recommendations

5.1. Conclusion

Breast cancer is the most commonly occurring cancer in women and the second most common cancer overall. Early detection is critical in reducing the mortality rate. Water-bath ultrasound breast scanning has the potential to be a screening method. At the TU Delft, a full-wave ultrasound inversion algorithm is available. This algorithm shows promising results for modelled data and phantom measurements. However, the currently available measurement system is not able to measure real human breasts.
For this study, there was the opportunity of measuring ex-vivo human breasts at the Pathology Department in the Erasmus MC. Using this opportunity two projects were executed. Firstly, an echo-scan of an ablation mamma is made and this scan is compared with its cross-sectional photograph. This contributes to more knowledge about the properties of a human breast and its characteristics when imaging it using ultrasound. Secondly, a water-cup setup is built to measure an ex-vivo human breast. The water-cup setup includes a Verasonics research ultrasound system, a plastic cup with a diameter of 9 cm, four acoustic windows and four phased array ultrasound probes that can transmit frequencies in the range from 1 to 4 MHz. Before the water-cup is used to measure real tissue, a phantom study is executed to test the operability of the water-cup setup.

The female human breast has a pudding-like texture with the glandular tissue heterogeneously spread inside. This makes it hard to slice the breast at the same position as the echo-scan; the structures inside the breast will be deformed when it is sliced. Therefore, it is difficult to find the glandular tissue structures, present in the cross-sectional photograph, back in the echo-scan. Also, it is seen that when the breast is cooled or put on formalin its properties change. When the breast is cooled it gets stiffer. When the breast is put on formalin during one night it gets stiffer and changes from colour.
To obtain an echo-scan that can be compared with its cross-sectional photograph, the ablation mamma should be big, minimal a cup-size 'C', and there should be skin on the breast. The acoustic coupling between the probe and the breast is better when the probe is pressed on the skin instead of putting it directly, with ultrasound gel in between, on fatty tissue.

A Synthetic Aperture Focusing Technique, an Algebraic Reconstruction Technique and a Born inversion algorithm are applied to the phantom-data of the water-cup. The built water-cup has difficulties to reconstruct a speed of sound map of the measured agar phantom. This is because the measurement-setup has spaces between the four probes that are not covered with transducers. From these areas, no signal can be sent and received. Also, obtaining the correct transmitted field is crucial for the application of inversion algorithms. Employing an incorrect incident field can cause artefacts in the final image.

The phantom study shows that for reconstructing a contrast image with reflection data using a Back-Propagation based algorithm, all transmitted frequencies are needed to build a proper image. Hereby a method is proposed that divides all the frequencies randomly over each source-receiver combination. This method decreases the computation time as each source-receiver combination no longer needs to analyse all frequen-

cies. The downside is the aliasing-noise appearing in the images. Furthermore, the difference between reflection and transmission signal is observed. This difference depends on the transmitted frequency and the object that is measured. It is shown that scaling the reflection data with the transmission data results in a better expression of the contrasts in the image. What is also noticed during the course of this project is that it is wise to first use a simpler algorithm (SAFT, ART) to make an image of the data and then turn to a more complicated algorithm (Born inversion). Most of the time, when a simpler algorithm is not capable to reconstruct a rough image, the more complicated algorithms won't be able to do so either.

The built water-cup is not able to make an image, in which the glandular tissue can be distinguished from the fat tissue, of an ex-vivo human breast. The breast can be distinguished from the water in which it lays. The elevation-resolution of the used probe makes structures in this direction 'blur out'. Because of the heterogeneous spreading of the glandular tissue in the breast, imaging the breast is a 3D problem.

5.2. Recommendations

For the ex-vivo human breast study, a better cross-sectional slice can be made when the breast is cooled before it is cut. Thus, first an echo-scan should be made and the position of the probe on the breast is marked, then the breast is dyed by the pathologist. After the dyeing, the breast should be cooled for 2 to 3 hours. When the breast is cooled it is stiffer. This makes it easier to make the cross-section at the position of the echo-scan.

The phantom that is used during this project exists out of agar, a straw and two wires. The straw and wires are not tissue-like objects, whereas they have a speed of sound that is much higher than the speed of sounds present in the breast. To test the applied algorithms more extensively, a new tissue-like phantom should be made. With materials that have a speed of sound in the range of the speed of sound of the breast.

The scaling of randomly picked reflections with transmission data gives promising first results. However, more research should be done on filtering out the noise caused by this type of frequency picking. In the end, the contrasts should be reconstructed with mainly the reflection data and the transmission data should be used to reconstruct a speed of sound map.

It is my belief that with the current knowledge about the structures inside the breast and the reconstruction algorithms, a new DBUS-system can be built. This setup should take the heterogeneous 3D structure of the breast into account. This can be done by constructing a half-spherical setup. Another possible setup can include two circular arrays that can move independently from each other. The system should transmit frequencies up to 1.5 MHz. This makes it possible to apply the available full-wave inversion technique. An initial image can possibly be made with a combined ART and SAFT algorithm. Also, these frequencies up to 1.5 MHz are theoretically capable of finding tumours down to 0.5 mm.

Bibliography

[1] WHO, "Breast cancer," 2012.

[2] IARC, "Breast cancer estimated incidence, mortality and prevalence worldwide in 2012," 2012.

[3] RIVM, "Breast cancer screening programme," 2011.

[4] N. Özmen, *Ultrasound Imaging Methods for Breast Cancer Detection*. PhD thesis, TU Delft, 2014.

[5] D. I. Bickle and D. N. Yang, "Breast ultrasound."

[6] N. Duric, P. Littrup, L. Poulo, A. Babkin, R. Pevzner, E. Holsapple, O. Rama, and C. Glide, "Detection of breast cancer with ultrasound tomography: First results with the computed ultrasound risk evaluation (cure) prototype," *Medical Physics*, vol. 34, no. 2, pp. 773–785.

[7] Roy, Schmidt, Li, Allada, West, Kunz, and Duric, "Breast imaging using ultrasound tomography: From clinical requirements to system design," in *2013 IEEE International Ultrasonics Symposium (IUS)*, pp. 1174–1177, July 2013.

[8] G. Sandhu, C. Li, O. Roy, Schmidt, and N. Duric, "Frequency domain ultrasound waveform tomography: Breast imaging using a ring transducer," *Physics in Medicine and Biology*, vol. 60, pp. 5381–5398, 06 2015.

[9] P. Pellegretti, M. Vicari, M. Zani, M. Weigel, D. Borup, J. Wiskin, U. Saueressig, E. Kotter, and M. Langer, "A clinical experience of a prototype automated breast ultrasound system combining transmission and reflection 3d imaging," in *2011 IEEE International Ultrasonics Symposium*, pp. 1407–1410, Oct 2011.

[10] J. W. Wiskin, D. T. Borup, E. Iuanow, J. Klock, and M. W. Lenox, "3-d nonlinear acoustic inverse scattering: Algorithm and quantitative results," *IEEE Transactions on Ultrasonics, Ferroelectrics, and Frequency Control*, vol. 64, pp. 1161–1174, Aug 2017.

[11] H. Gemmeke, T. Hopp, M. Zapf, C. Kaiser, and N. V. Ruiter, "3d ultrasound computer tomography: Hardware setup, reconstruction methods and first clinical results," *Nuclear Instruments and Methods in Physics Research Section A: Accelerators, Spectrometers, Detectors and Associated Equipment*, vol. 873, pp. 59 – 65, 2017. Imaging 2016.

[12] H. Gemmeke, L. Berger, T. Hopp, M. Zapf, W. Tan, R. Blanco, R. Leys, I. Peric, and N. V. Ruiter, "The new generation of the kit 3d usct," in *Proceedings of the International Workshop on Medical Ultrasound Tomography: 1.- 3. Nov. 2017, Speyer, Germany. Hrsg.: T. Hopp*, pp. 271–282, KIT Scientific Publishing, Karlsruhe, 2018. 54.02.02; LK 01.

[13] L. Huang, J. Shin, T. Chena, Y. Lin, K. Gao, M. Intrator, and K. Hanson, "Breast ultrasound tomography with two parallel transducer arrays," in *Proceedings of SPIE*, vol. 9783, pp. 9783 – 9783 – 12, 2016.

[14] K. J. Opieliński, P. Pruchnicki, P. Szymanowski, W. K. Szepieniec, H. Szweda, E. Świś, M. Jóźwik, M. Tenderenda, and M. Bułkowskif, "Multimodal ultrasound computer-assisted tomography: An approach to the recognition of breast lesions," *Computerized Medical Imaging and Graphics*, vol. 65, pp. 102 – 114, 2018. Advances in Biomedical Image Processing.

[15] M. Ding, J. Song, L. Zhou, S. Wang, and M. Yuchi, "In vitro and in vivo evaluations of breast ultrasound tomography imaging system in hust," in *Proceedings of SPIE*, vol. 10580, pp. 10580 – 10580 – 8, 2018.

[16] L. Medina-Valdés, M. Pérez-Liva, J. Camacho, J. Udías, J. Herraiz, and N. González-Salido, "Multi-modal ultrasound imaging for breast cancer detection," *Physics Procedia*, vol. 63, pp. 134 – 140, 2015. 43rd Annual UIA Symposium 23-25 April 2014 CSIC Madrid, Spain.

[17] T. Hopp, N. Ruiter, J. Bamber, N. Duric, and K. van Dongen, *Proceedings of the International Workshop on Medical Ultrasound Tomography: 1.- 3. Nov. 2017*. KIT Scientific Publishing, 2018.

[18] R. Govers, "Generation and validation of an anatomically realistic numerical phantom for breast ultrasonography," Master thesis, Erasmus MC & TU Delft, 2018.

[19] D. Gisolf and E. Verschuur, *The principles of quantitative acoustical imaging.* EAGE Publ., 2010.

[20] O. Werner, "Ultrasound computed tomography using algebraic reconstruction technique," Bachelor thesis, TU Delft, 2017.

[21] A. Ng and J. Swanevelder, "Resolution in ultrasound imaging," *Continuing Education in Anaesthesia Critical Care Pain*, vol. 11, no. 5, pp. 186 – 192, 2011.

[22] S. Rajagopal, N. Sadhoo, and B. Zeqiri, "Reference characterisation of sound speed and attenuation of the iec agar-based tissue-mimicking material up to a frequency of 60 mhz," *Ultrasound in Medicine and Biology*, vol. 41, pp. 317–333, 2019/01/19 2015.

[23] T. Kondo, S. Kishimoto, and Y. Sato, "Acoustic properties of plastics for applications to probes of an ultrasonic diagnostic instrument," *Japanese Journal of Applied Physics*, vol. 31, no. S1, p. 163, 1992.

[24] A. B. Ramirez and K. W. A. van Dongen, "Can sources and receivers be interchanged for imaging?," in *2016 IEEE International Ultrasonics Symposium (IUS)*, pp. 1–4, Sep. 2016.

[25] W. Hu, J. Chen, J. Liu, and A. Abubakar, "Retrieving low wavenumber information in fwi: An overview of the cycle-skipping phenomenon and solutions," *IEEE Signal Processing Magazine*, vol. 35, pp. 132–141, March 2018.

[26] E. Scherders, "Generation of an acoustic breast model from a cross-section of an ablatio mamma," Bachelor thesis, TU Delft, 2018.

[27] W. Marczak, "Water as a standard in the measurements of speed of sound in liquids," *The Journal of the Acoustical Society of America*, vol. 102, no. 5, pp. 2776–2779, 1997.

A

Scaling of reflection with transmission data

Figure A.1 shows back-propagation images in which the reflection data is scaled using various λ-factors. In image (b), the λ-factor is obtained by dividing the maximum absolute amplitude of a transmission data a-scan with the maximum absolute amplitude of a reflection data a-scan; λ=24.4. In image (c), the λ-factor is obtained by dividing the energy of a transmission data a-scan with the energy of a reflection data a-scan; λ=5.9.

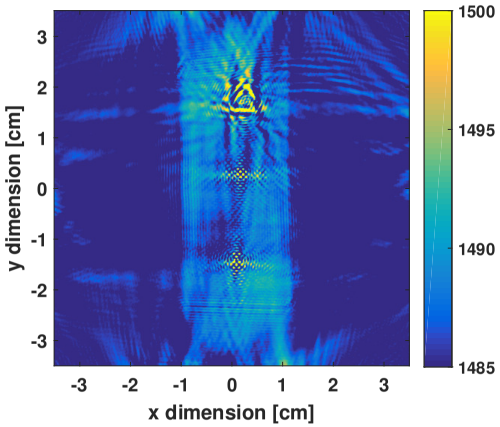

(a) Born inversion image of phantom with 10 frequencies from 1.3 to 1.4 MHz of the reflection and transmission data used to reconstruct image

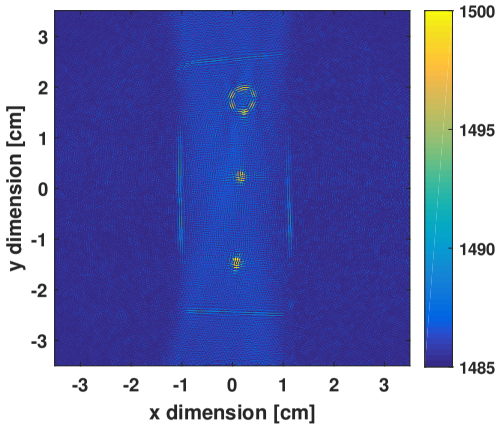

(b) Same configuration is used to reconstruct image (b) as image (a), only the reflection data is scaled with the transmission data with λ=24.4. For the reflection data there are for each source-receiver combination 10 frequencies randomly picked in the range of 0.6 to 2.49 MHz

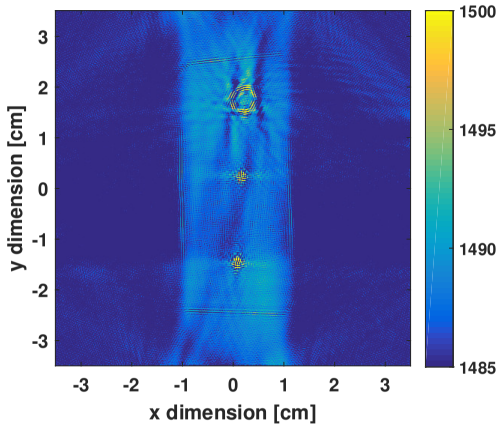

(c) Same configuration is used to reconstruct image (c) as image (a), only the reflection data is scaled with the transmission data with λ=5.9. For the reflection data there are for each source-receiver combination 10 frequencies randomly picked in the range of 0.6 to 2.49 MHz

Figure A.1: Born inversion images of the straw-wire phantom; in image (b) the reflection data is scaled with the transmission data and for the reflection data 10 frequencies are randomly chosen for each source-receiver combination

B

1 frequency BI image

The images in Figure B.1 are constructed using a Born inversion algorithm that uses only one frequency for each source-receiver combination. Also, a λ scaling factor of 5.9 is used.

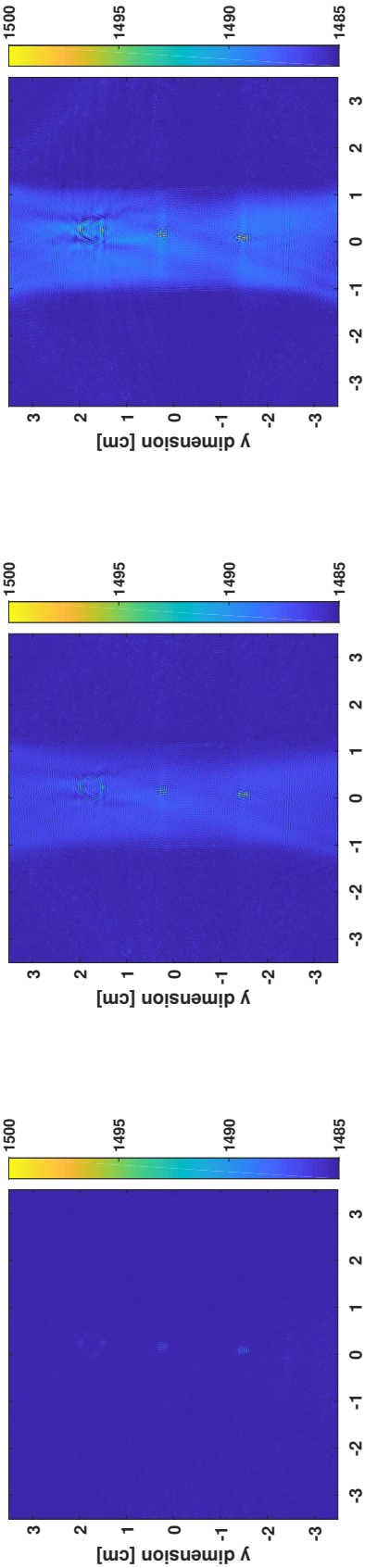

(a) Born inversion image of phantom, after one iteration, constructed with 1 frequency

(b) Born inversion image of phantom, after eight iterations, constructed with 1 frequency

(c) Born inversion image of phantom, after twelve iterations, constructed with 1 frequency

Figure B.1: Born inversion images of the straw-wire phantom. One frequency for each source-receiver combination is used to construct an image. For reflection data the frequencies are randomly chosen in the range from 1.2 to 2.3 MHz and for the transmission data the 1.3 MHz frequency is analyzed.

C

SAFT images for various probe configurations

Figure C.1 shows SAFT images for various probe configurations. Per probe there are 24 sources used and all transducers work as a receiver. Thus the number of used transducers increases when adding an extra probe.

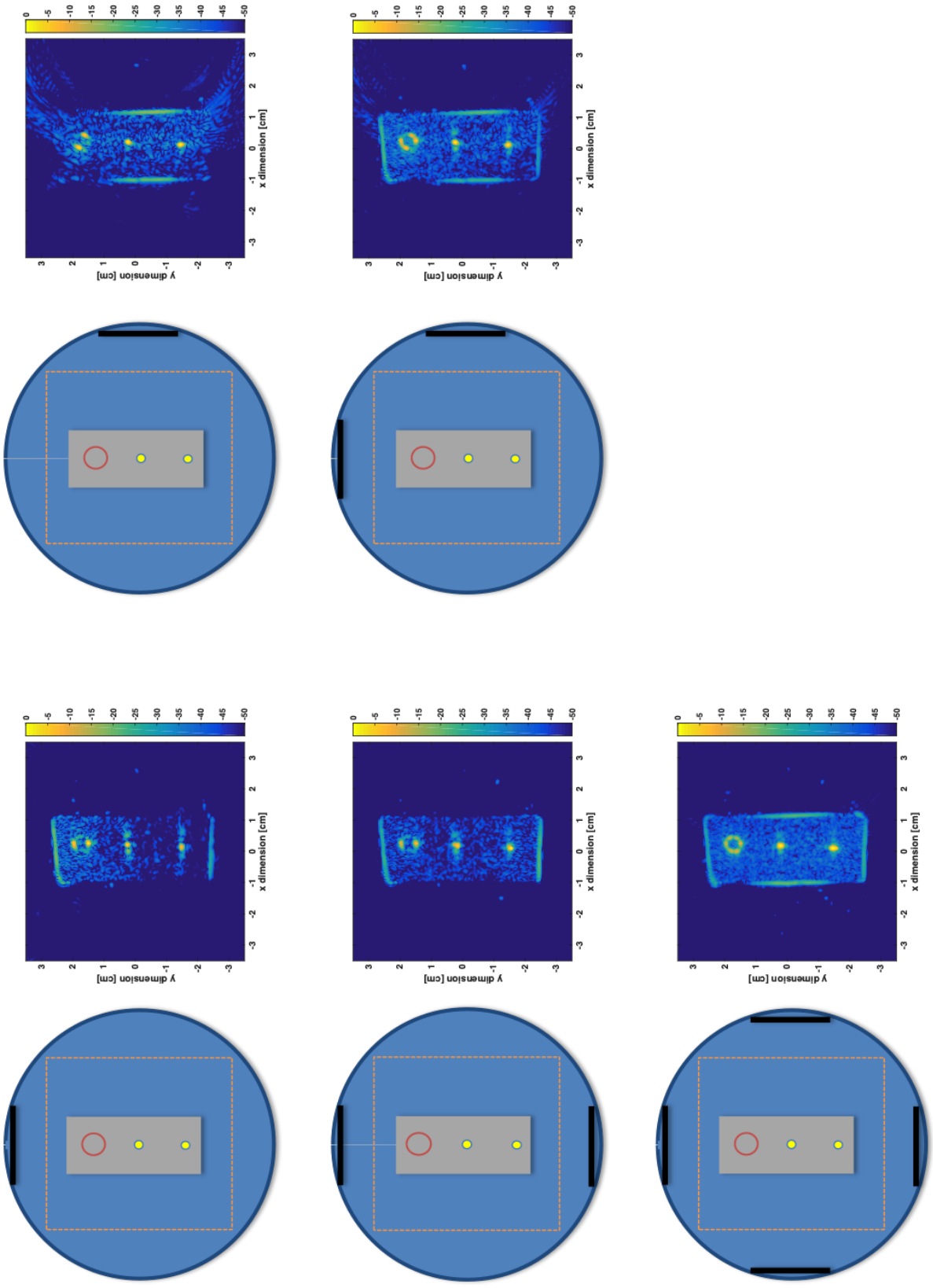

Figure C. 1: SAFT images of the straw-wire phantom for different probe configurations of the water-cup setup